Impedance Measurement of Cells; Experiment and Analysis of Passivation Layer

Shree Narayanan Sreedharan Nair

Thesis submitted to the faculty of the Virginia Polytechnic Institute and State University
in partial fulfillment of the requirements for the degree of

Master of Science
In
Electrical Engineering

Masoud Agah (Chair)
Kathleen Meehan
Rafael Davalos

20th of November, 2009
Blacksburg, Virginia

Keywords: bio-impedance, modeling, analysis

Impedance Measurement of Cells; Experiment and Analysis of Passivation Layer

Shree Narayanan Sreedharan Nair

ABSTRACT

Biological cells like any other material do conduct electricity. Though they come across as insulators, the resistance to the flow of current, i.e. impedance, could be used to characterize the cell itself. In this aspect, the impedance of cells can be a promising tool to investigate the state of the cell.

A simple way of measuring the impedance would be a planar-microelectrode method. The cells are contained in culture medium while measurements are taken with micro-electrodes fabricated on top of a substrate. Since both the probe "tips" do not come in contact with the probed object, the impedance to be measured includes some components apart from that contributed by the cells.

There have been publications reporting the usage of impedance of a cell to determine changes in the state of cells due to healing, drug candidate testing, functional genomic studies and so on.

In this thesis, an effort has been made to measure the impedance of cells. Further, a component of the sensor, the passivation layer has been investigated for its contribution to the measured impedance in a quantitative manner.

To my parents for having supported me in every decision I have taken and to God who has brought me to where I am right now

ACKNOWLEDGEMENTS

I should thank Dr. Masoud Agah, Director, VT MEMS and my advisor, who provided me this opportunity. I have learned from him, the need of being able to present data in the right manner. Doing research and presenting it in the right manner are two different aspects, I believe.

I should also thank Dr. Kathleen Meehan and Dr. Rafael Davalos for agreeing to be on my committee and providing me with valuable inputs, irrespective of the project for which advice was requested.

My deepest acknowledgements to Dr. Jeannine Strobl and Dr. Elankumaran Subbiah (College of Veterinary Medicine) who have helped me with cell culturing and provided valuable information when I was in dire need. Mr. Gopakumar Moorkant at ILSB, needs to be specially mentioned for culturing cells for me and allowing me to observe them at their facilities, in spite of his hectic schedule. Some of their remarks threw light on a field which was alien to me and some observations made on those cell-cultures were highly valuable to me and am sure will be employed some day for a greater use. Don Leber, Manager of the MicrON clean room, has always ensured that the machines were operational and has always been there to respond to our SOS calls.

In an academic setting, not only the faculty but fellow labmates can play a huge role in your research and not lesser than Mehdi Nikkhah. A hardworking student, he was the first person with whom I worked and definitely leads the way, with new results always at his disposal to be submitted for review. He handled the cell-culturing part for most of the experiments relieving me of a lot of work. Bassam Alfeeli, the senior most in our lab is the best person to speak to, research related or otherwise. Current students Liam Renaghan, Phillip Zellner and Vaishnavi S and former students Syed Ali and Amin Zareian always made the lab a better place to be in, than home. Graduate Students at WML, Krishna Vummidi, Parrish Ralston, Nikhil Kakkar and Marcus Oliver have been a good bunch to discuss with when I needed to let my thoughts flow out and have some reliable feedback. Theirs has been my most frequented place apart from my lab.

Having contributed my 5 cents to this budding research in our lab, I am happy that I have been given a chance to contribute further in another project. I am looking forward to work with the faculty at Tech, and all my Graduate friends, enjoying my research and life equally.

May God bless all of us in our endeavors.

Contents

List of Figures

List of Tables

1 INTRODUCTION

Interacting with cells (or tissues) in the electrical domain has been in practice for a long time. There are many reports which pre-date the first publication that monitored cells based on their impedance [6-9]. In a 1983 publication, impedance was identified to be a useful tool in determining the condition of cells [10]. However, the work done so far has been geared towards attachment and spreading of cells on electrodes for which it is ideally suited. It is possible that the response of the cells can be modified by bioengineering the environment for selectivity.

Measuring the impedance has been shown to be capable of monitoring attachment, spreading of cells to different surfaces, effect of chemicals such as kinase, trypsin, cytochalasin B, wound healing, micromotion, changes in the pH of medium due to periodic injection of CO_2 in an incubator, response of immune system to parasites, and functional genomic studies [11-14]. This extensive list of studies demonstrates the promise of bio-impedance measurement and analysis as an alternative approach to the time-tested visual-observation based analysis.

Impedance of an object is determined by contacting its "two terminals" to the two terminals of a measurement unit. In the case of a cell which can roughly fit into a box that measures 30μm on an edge, probes of similar dimension need to be fabricated such that a cell can be accommodated on both probes. Moreover, cells need to be within culture medium to ensure their viability. In the process, the electrodes are exposed to the culture medium and the impedance measured is contributed by the cells as well as the culture medium. This is a very simple picture of how one can measure the impedance due to cells.

The presence of culture medium is alone not sufficient to ensure viable cells. Hence, we move this setup into an incubator which will maintain the environmental conditions for culturing our cells. This will enable *in-vitro* measurements to be taken over a long time. By studying the measurements from this cell-culture, it is possible to study the cell.

The reasons micro-fabricated sensors are suitable for this study, apart from the dimensions of cells, are the inherent advantages of micro-systems. These are small sensors which are batch-fabricated. For example, we fabricate 12 sensors on a 4" wafer. Yield-wise, we could recover all of them in most cases. Batch-fabrication helps to keep down costs since all these devices are fabricated at the same time. In addition, each device could have multiple sensing sites. In our case, we have 8 sensing sites in a device. We were restricted by the limitation of having large bond pads to solder wires for interfacing rather than wire-bond. Multiple sensing sites, in turn, enable us to probe at multiple points and collect statistically significant information which is important to prevent false-negatives (and false positives) when making decisions.

Silicon is chosen as the substrate and photoresist as the passivation material. The aim was to reduce the extent of manual intervention in the fabrication flow. For example, previous endeavors have involved specific steps such as placing a cover-glass with red-wax and painting with epoxy [12, 15]. However, in our work, these were avoided to realize a true batch-fabricated design. There are drawbacks, as well, to this decision. Silicon tends to have more parasitic capacitance.

On the whole, batch fabricated micro-impedance sensors have a tremendous potential to be commercially implemented for the larger benefit of the society. However, it needs patience,

creativity in bio-engineering responses and meticulousness in obtaining repeatable results to take it another step forward.

2 LITERATURE SURVEY

The first recorded measurement of the impedance of cells using this method was made in 1984, by Giaever (a 1973 Nobel Laureate) and Keese [3]. They monitored human embryonic lung fibroblast cell line and its transformed equivalent, WI-38 and WI-38 VA13. The electrical impedance measured was related to the physical state of the cell. The structure in Fig 2-1 describes their sensor. It consisted of gold micro-electrodes fabricated on polystyrene dishes. The amplitude of the response was related to the adherence, spreading and attachment of cells onto the electrode. When Cytochalasin B was added, a chemical which affects cell motility, the fluctuation in the output was observed to be affected as well. In a subsequent paper, in 1986, they processed the signal obtained from the measurements comparing it to a "random walk" model [12]. In this manner, they processed the signal digitally to remove small fluctuations that are characteristic to cell-motion. However, on an average, the trend was shown to be reproducible.

They named this technique as "Cell-Substrate Impedance Sensor" (CIS) in a 1990 paper

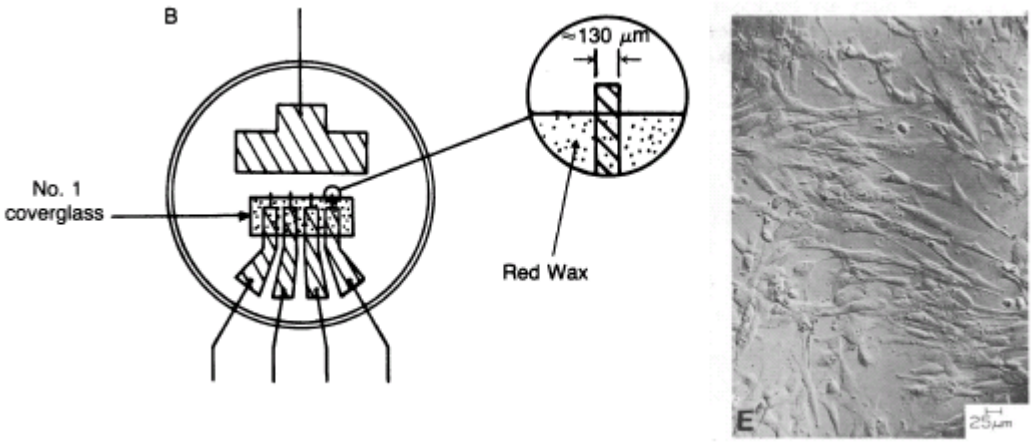

Fig 2-1 An image of the sensor (left) fabricated by Giaever et. al. and a confluent cell layer (right). [3].

[16]. In a subsequent paper, they modeled the cell layer with capacitance corresponding to top

and bottom membranes (C_m) and a resistance that corresponded to the gap between the cells and substrate [13]. Since, majority of cell surface is not in contact with the substrate, the corresponding resistance can be significant. By deriving equations corresponding to this structure and solving them, they related the specific impedance of the medium-exposed electrode, cell-covered electrode and the above 3 parameters. By substituting the data, they obtained values of cell-substrate gap anywhere between 13nm to 285 nm depending on the assumed geometric shape of the cell and type of the cell being used. This has been compared with values of 10 nm – 30 nm reported using interference reflection microscopy for chick heart fibroblasts [17]. This was the first instance of modeling a non-invasive automated electronic technique to monitor cell attachment and motility.

Mitra et. al. from the same group , related the fractional area coverage of electrodes to the impedance measured by the same method [18]. They employed a multiple well dish to “fix” cells at different times and determine the coverage of electrodes. They found a correlation between these two quantities, for the measured and the simulated data from the theoretical model previously mentioned.

In 1993, Giaever and Keese were awarded a patent for a measurement assay on the same principle to “measure cell spreading and motility”, titled “Cell Substrate Electrical Impedance Sensor with Multiple Electrode Array” [19].Their method used a passive matrix to switch the necessary sensing site. Renamed as “Electrical Cell-Substrate Impedance Sensing” (ECIS), it was later used to analyze the motility and spreading of epithelial cells from canine kidney (MDCK) [14, 20]. The method in its entirety for the first time appeared in the NATO ASI Series print edition [21].

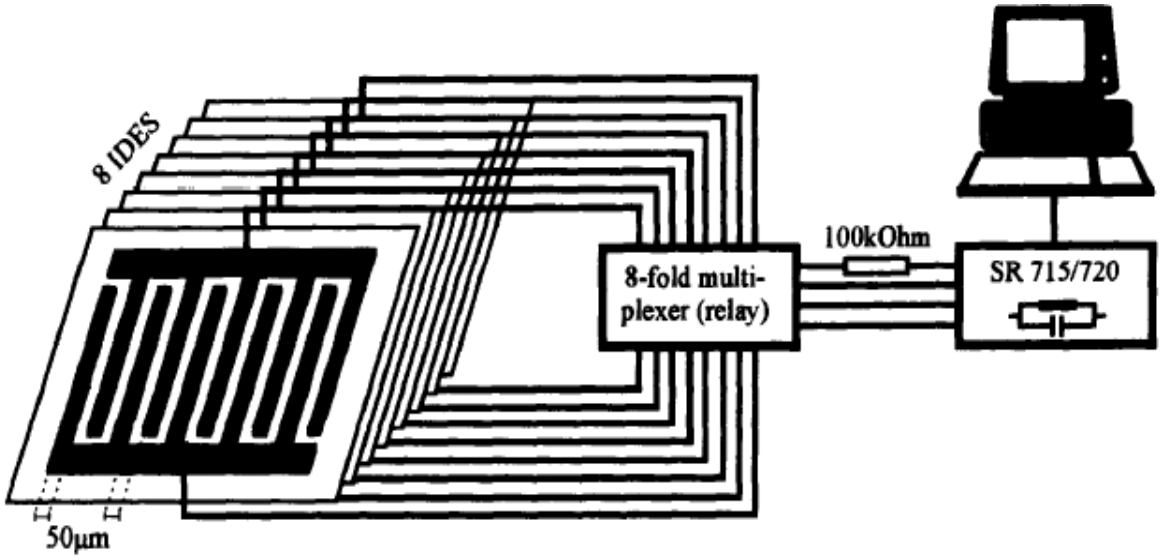

Fig 2-2 A schematic of the setup used to multiplex 8 IDES sensors in a computer controlled environment. [5].

The first improvement to the impedance measurement method came in 1997 when Ehret et. al. from Germany published results of impedance measurements from "Inter-Digitated Electrode Structures" (IDES) [5]. As the name suggests, this consists of two inter-digitated platinum electrodes on a sapphire substrate. A "trough" made from epoxy was used to isolate the 5mm square sensing area. By using 8 such sensors, shown in Fig 2-2, connected in parallel and multiplexed for measurements, the effect of toxic Cd^{2+} on animal cells was reported for different Cd^{2+} concentrations. Elsewhere, ECIS was used for measurement of Transepithelial resistance, comparison study of MDCK and WI-38 cells, and was published in print edition books [22-24]. ECIS sensors are now available as a commercial product from Applied BioPhysics, NY, USA.

Impedance measurement based micro-bio-sensor research took a significant leap with results published by a group under Dr. David Greve at CMU, Pittsburg. In a 2003 paper, Greve et. al. modeled the electrical equivalent of the impedance being measured, related it to the area of the electrode [25]. Simulations were performed for the metal-electrolyte interface on the basis of the structure of the double-layer that was described. The increase in the impedance in the presence of cells was explained in terms of the cell-substrate gap and coverage area of the electrode [26-28].

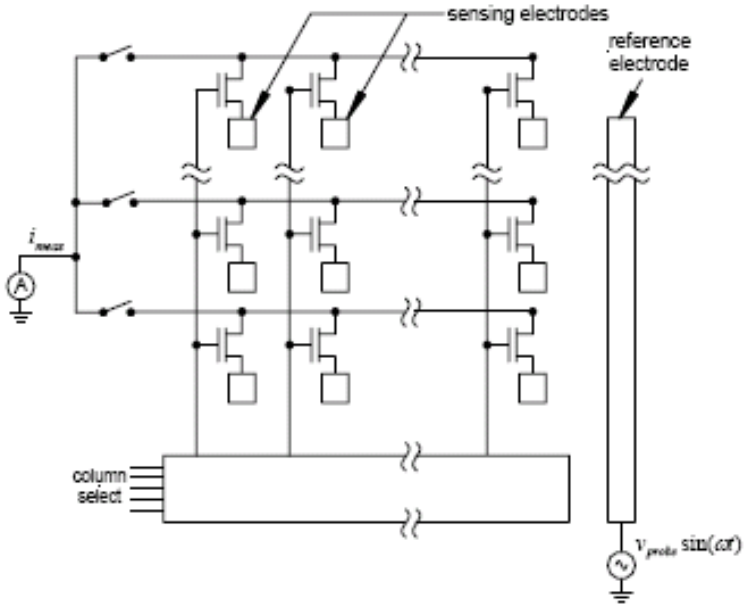

Fig 2-3 The active matrix proposed by Huang et. al. for measuring the impedance from multiple sensing sites [2].

Huang et. al., from the same group, reported the fabrication of an array of sensing sites (Fig 2-3) which are switched using on-chip transistors (active elements) fabricated in the AMI 1.5µ technology [2]. Their experiments were performed on 3T3 fibroblasts and human carcinoma cells [11, 29].They also had an initiative to fabricate the same array, in collaboration with Lehigh university, using a TFT process that used glass or plastic as a substrate. Images of both devices are shown in Fig 2-4. The reason for choosing TFT was the presence of aluminium (non-bio-

compatible) in the CMOS technology process that they were using. They worked around this drawback by using electroless gold plating onto the exposed aluminium. It can be noted that using plastic as substrate would have resulted in larger open-circuit impedance compared to silicon. However, they ran into problems with "passivation pin-hole defects" and transistor gate leakage current.

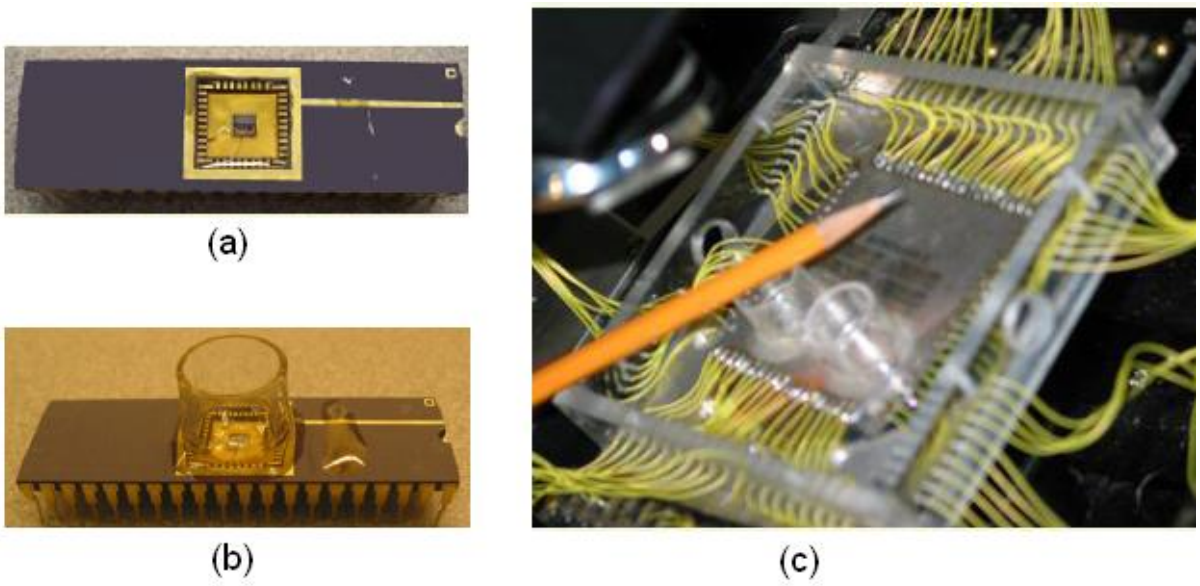

Fig 2-4 CMOS Technology based active-matrix based impedance sensing array (a) before and (b) after packaging. Thin Film TFT based array. From [2] and the corresponding conference presentation accessed from http://www.ece.cmu.edu/~dwg/research/ECS2005invited.pdf on Nov 16,2009.

Hoffman et. al. changed the approach of using impedance as a physical indicator, by insulating the electrode altogether from the solution using a 10μm Parylene-C layer [30]. The intention was to track down the properties of a bulk solution that is above the insulation layer. The fermentation process of the complex medium YPG in the presence of the yeast *Hansenula Polymorpha* changes the electrical properties of the medium which was measured using the electrodes. Alternatively, a polyimide film attached to the base of a micro-titer plate with

electrodes fabricated underneath has been reported [31]. A two-electrode measurement technique was reported to be sufficient to monitor the fermentation process.

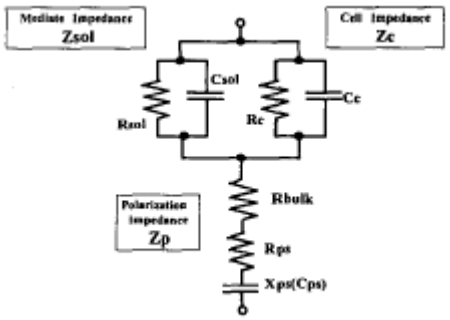

Fig 2-5 The equivalent circuit used by Goda et. al. to explain measurements through simulations [4].

Elsewhere, there have been attempts to explain "possible effects" due to different physical conditions such as area coverage, scaling factor by modeling the impedance using different models [32, 33]. A notable publication by Goda et. al., analyzed the electrical measurements from the ECIS system and simulated the effect of changing solution resistance and cell-to-cell substrate distance on the overall measurements [4].

In a 2004 paper, Gomes et. al. published results of analyzing the interaction between immune cells and parasites [34]. The intention was to analyze the clustering of parasitic *Perkinsus atlanticus* in the presence of a hemocyte. Using interdigitated electrodes and another large electrode on top, measurements made either among the parallel electrodes on the same plane or against the large electrode on top was reported. As the cells clustered, the response was found to increase and the peak shifted depending on the measurement option chosen.

Impedance measurement technique was reportedly used to detect the presence of *E.Coli.*in food material. Radke et. al. fabricated an impedance sensor and coated the sensor surface with antibodies capable of immobilizing the bacterium [35]. Apart from having a

reasonable lower detection limit of 10^5 CFU/ml, the response time was very quick and was measured to be within 5 minutes.

Among other designs used for measuring the impedance due to cells, Rahman et. al. have measured the response of HUVEC cells [36]. Price et. al. experimentally determined that a value of 5.5 for the ratio of the coating area to coating thickness can remove the effect of the coating layer on the impedance [37].

3 ELECTRICAL STRUCTURE

3.1 CPE as a circuit element

An application note from Gamry Instruments, available in the public domain on their webpage, is a useful reference for basic electrical concepts [38]. One of the fundamental reactive circuit elements is a capacitor whose impedance can be modeled as in Eq 3.1. It can be observed that the phase of this element is fixed at -90˚ and a log-log plot of the magnitude of the impedance against angular frequency, will have a slope of -1.

$$Z = \frac{1}{j\omega C} = \frac{1}{\omega C} * e^{-j\pi/2} \tag{3.1}$$

However, in reality, measurements of capacitive elements do not follow the ideal frequency relationship. It will be seen later that the phase angle of the capacitor will be constant but not equal to -90˚. While the reason has been up for debate, one theory attributes this behavior to the surface roughness that leads to a transmission line like effect.

This non-ideal circuit element is defined as a Constant Phase Element (CPE). It is a circuit element which consists of frequency dependent resistive and reactive parts. While there are multiple way of defining this element we will take the definition in Eq. 3.2 [39].

$$Z = \frac{1}{\left(j\omega C_{coeff}\right)^n} = \frac{1}{\left(\omega C_{coeff}\right)^n} * e^{-jn\pi/2} \tag{3.2}$$

In this definition, we have an additional parameter, “n” (0<n<1), defined as the phase exponent and C_{coeff} is a constant. It should be noted that C_{coeff} is an analogue of an ideal capacitance but does not have the same units. This parameter plays a role in the magnitude and

phase plot of the CPE. The phase plot is not fixed at -90˚ but at a value slightly lesser. Similarly, the slope of the log-log plot of the magnitude against angular frequency will be fixed at "–n".

3.2 Sensing arm

In a bio-impedance chip using the planar impedance measurement, the two electrodes lie flat on a surface as shown in the layouts in Fig 5-1 and Fig 5-3. The electrodes are thus exposed or "wetted" by the culture medium. This culture medium is an electrolyte consisting of conductive ions. Any metal-electrolyte interface is associated with interfacial impedance. Thus, the circuit path can be traced from one of the electrodes through its interfacial impedance, electrolyte solution and finally reaching the second electrode through its interfacial impedance.

The interfacial impedance is modeled as a double layer capacitance in parallel with Faradaic impedance. The origin of the double layer capacitance lies in the re-arrangement of ions that occurs in the liquid and is in the order of 20-40 $\mu F.cm^{-2}$[40]. This is the dominant component in moderate frequency AC response [1]. The electrode is either rich or deficient in electrons due to its high conductivity. Hence, some of the ions in the solution drift and align along a thin layer just next to the electrode based on their polarity. These layers of charges, on the electrode and in the solution, correspond to a parallel plate capacitor called as Helmholtz capacitor (C_H) with a separation of ~2 Å. This is also the origin of the term double layer.

However, this model does not explain the relation between capacitance and applied voltage that is observed experimentally and the change in capacitance due to dilution. The variation due to voltage was fixed by modeling the layer to be diffuse in nature, called as Gouy-Chapman Layer (C_G). However, this model deviated from the experimental values of capacitance at high concentration.

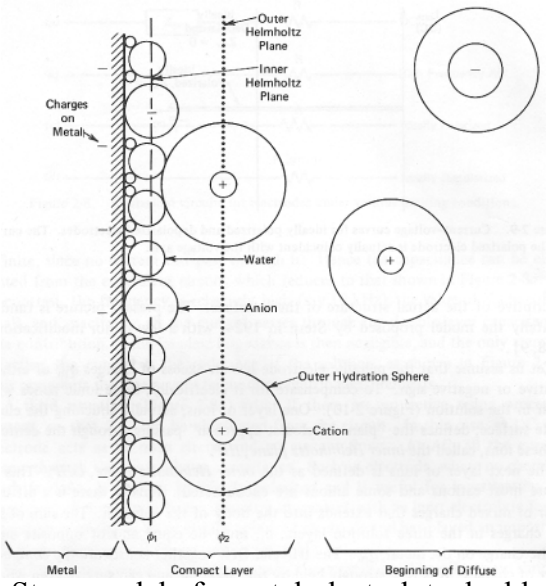

Fig 3-1 A Stern model of a metal-electrolyte double layer[1].

To fix the deficiency in the above models, Stern proposed an alternative, wherein the interfacial capacitance consisted of a fixed layer of charges, ~10^{-7} mm in width, and a diffuse layer that extends farther into the solution to a maximum of 10^{-3} mm. This Stern model (C_S) is sufficient to explain the interfacial capacitance in most cases and can be explained by Eq. 3.3 in most cases [40]. Depending on the concentration, either C_H or C_G is dominant.

$$\frac{1}{C_S} = \frac{1}{C_H} + \frac{1}{C_G} \tag{3.3}$$

In our case, we shall model this double layer capacitance to be proportional to the area of the electrode as in Eq. 3.4.

$$C_{dl} = C_{coeff}{}' * A \tag{3.4}$$

The double layer itself is modeled as a CPE.

$$Z_{dl} = (j\omega C_{dl})^{-n} \tag{3.5}$$

Having seen the origin of the interfacial capacitance, we now turn our attention to the Faradaic impedance. This is the only component that responds to DC excitation and is responsible for the chemical reaction that takes place at the electrode. For an electrode where no redox reaction takes place, Z_{far} is infinite in value and corresponds to a polarized electrode [41]. This can be split into two elements, namely the Charge transfer resistance and the Warburg impedance. Charge transfer reaction accounts for the transfer of electrons across the interface by changes in the oxidation state of the metal. In our measurements, at the frequencies under consideration, it will be observed that this element cannot be measured. Warburg impedance represents the impedance due to diffusion and has a characteristic -45˚ phase[42]. Faradaic impedance is large enough for most of the experiments in this research and only the Warburg impedance has been noticed in the measurements especially in the case where the entire surface is passivated. The Faradaic impedance is non-linear as it is dependent on the applied voltage [1].

Apart from these interfacial impedances, there exists a spreading or constriction or solution resistance. When current flows out of an electrode into a large electrolyte, it encounters a characteristic resistance which is inversely proportional to the area of the electrode. This is modeled as given in Eq. 3.6, where 'ρ' is the resistivity of the solution and 'a' is the radius of the electrode. '1/ρ', the conductivity of the culture medium in use was measured to be 13.1mS/cm using a conductivity meter.

$$R_{sp} = \frac{\rho}{4a} = \frac{R_{spcoeff}}{Area^{0.5}} \tag{3.6}$$

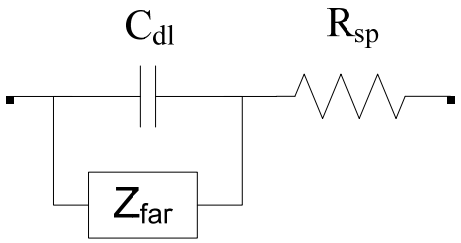

Fig 3-2 Randles model to represent the impedance of a solid-liquid interface

Based on the double-layer and solution resistance explained above, we can now model the metal-electrolyte interface, called as "Randles model" shown in Fig 3-2 [43]. Fig 3-3 shows the variation of the magnitude of the impedance of the metal-electrolyte interface with varying area. The impedance due to the presence of cells (Z_{cell}) on the electrode will appear in series with the interfacial capacitance and is modeled as a simple parallel RC circuit, wherein C is actually a CPE. As electrode area increases, interfacial impedance reduces. The impedance due to cells will also decrease and the spreading resistance will dominate, since it decreases only by the square root of area. This is not preferable and large electrodes are not advisable.

As seen above, larger the area of the exposed electrode, the smaller the impedance. It is preferable to measure the impedance due to the cells on one among the two electrodes across which the impedance is being measured. Hence, the area of one of the electrode is made large enough, called as the common counter-electrode. Since its impedance is small when compared to the other electrodes, we will measure the impedance between every electrode and the common counter-electrode.

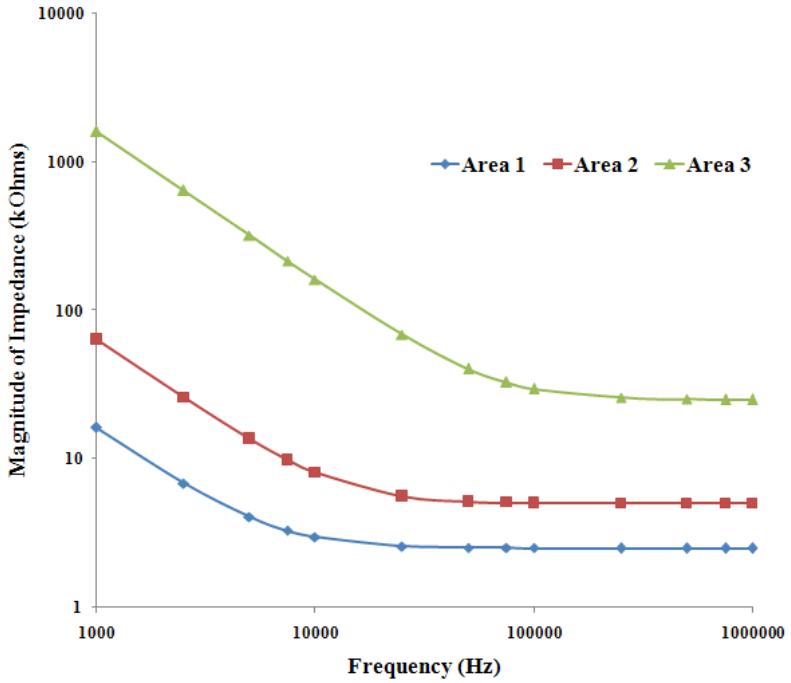

Fig 3-3 Simulated values of impedance of electrode for varying areas. $Area_1 > Area_2 > Area_3$

3.3 Passivation arm

It can be observed that there exists an electrical path through the passivation layer and the solution [44]. The impedance due to the passivated area (Z_p) can be modeled as a capacitance in parallel with Warburg impedance (Z_w). The Warburg impedance is due to diffusion limited reaction at the interface and has a characteristic -45˚ phase and can be seen at low frequencies in the phase plot of Fig 6-12. This capacitance is a Constant Phase Elements (CPEs) which is observed in the measurements.

3.4 Complete electrical equivalent

Apart from the sensing and passivation arm there exists a parasitic capacitance (C_{par}) which is seen in the measurements as well. We can attribute this to capacitors such as the substrate and solution capacitances which have not been included in the previous two sections. The final equivalent circuit model is shown in Fig 3-4.

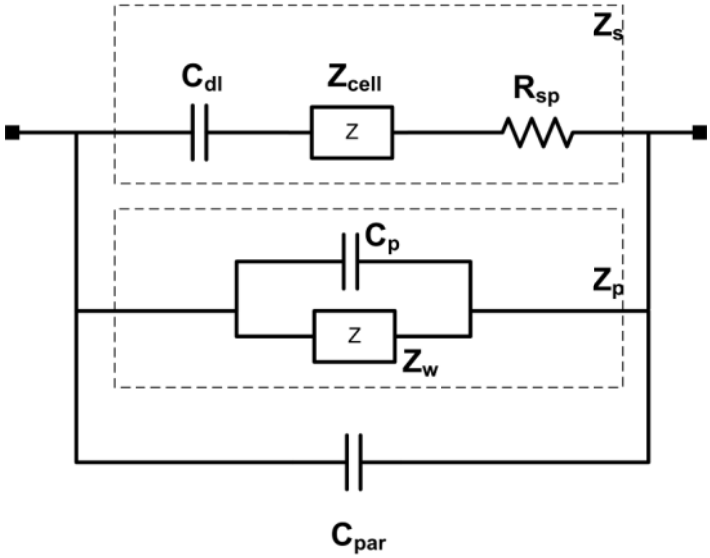

Fig 3-4 The complete electrical equivalent for the sensor.

4 MEASUREMENT SETUP

In order to measure the impedance of cells, we use an HP4192A impedance analyzer. An impedance analyzer measures the impedance (magnitude and phase) by the application of an ac excitation. In this particular case, the measurement is based on auto-balancing bridge method. By connecting this instrument to a USB-GPIB port, automated recording of huge amounts of data for analysis can be made.

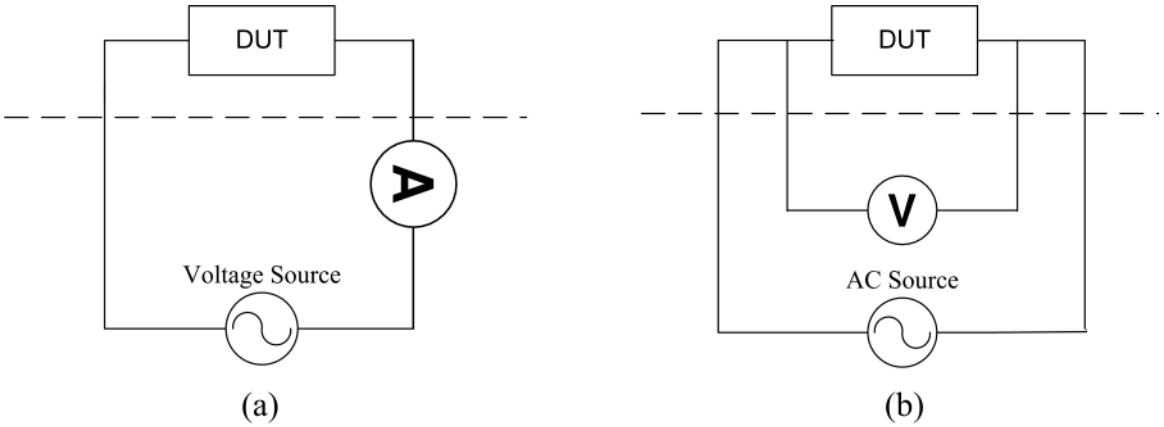

Fig 4-1 (a) 2-point and (b) 4-point probe impedance measurement comparison

Impedance measurement of a device-under-test (DUT) can be of two configurations, viz. two- and four-probe as shown in Fig 4-1. In a 2-probe measurement, the current sense and the voltage measurement are in series, and hence, contact and interconnect resistances will be included in the measurement. This error can be ignored if the resistance of the DUT is significantly larger than the sources of error [45]. If not, one can perform a 4-probe measurement. Notice in Fig 4-1 that the current carrying and voltage measuring terminals are on separate arms until the DUT, where they come in contact. In this manner, the interconnect resistance can be removed. The HP 4192A, which can perform 4-point measurement ability, has four terminal output terminals, namely Hp, Hc, Lp, Lc. To measure the impedance of a two

terminal device-under-test (DUT), Hp-Hc pair needs to be connected to one terminal and Lp-Lc pair need to be connected to the other terminal. It should be noted that the DUT in this case should not be grounded for proper measurement [46]. The output terminals are co-axial which provides sufficient shielding and noise immunity. The cells need to be cultured in an incubator for *in-vitro* measurement of the impedance. The coaxial cables in a 4-probe measurement setup are ideally suited to run over long distances.

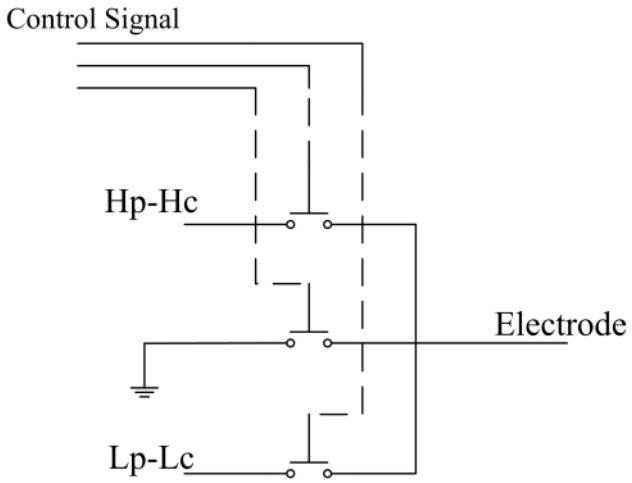

Fig 4-2 A group of 3 relays to switch a single electrode to one among three signals. There are 3 signals for each such group – PCB-C

The advantage of micro-fabricated bio-impedance sensors is the ability to have multiple sensing sites. However, to make multiple measurements, a multiplexer is necessary to use the same impedance analyzer across all the sites. The multiplexing on these boards is done by SPST (Single Pole Single Throw) Reed relays from Radioshack. Reed-relays are known for their fast-switching response and longer lifetime since they are hermetically sealed [47]. While requiring a larger footprint, electro-mechanical relays are, in general, preferable since they have better electrical isolation between their control and signal terminals when compared to solid-state relays. A PCB (printed circuit board), which will be denoted as PCB-C, with 13 groups of 3 relays was designed for switching the electrodes shown in Fig 4-2.

This single layer PCB had traces on both sides. The coaxial cables from impedance analyzer were connected to the traces on the board using a BNC-SMA adapter. The traces on the board were co-planar in fashion to minimize the crosstalk. Each group of 3 relays had 3 inputs, respectively as Hc-Hp, Lc-Lp, and GND (ground). The output of all 3 relays were tied together and in turn connected to one of the electrodes on the chip. Thus, each electrode can be switched to connect to either Hc-Hp or Lc-Lp or GND. A single SPST switch was used with one bit line as a control signal and each group/electrode used 3 bit lines.

The control signals for the multiplexer needed to be controlled from the computer. This enabled multiple frequency sweeps at regular intervals without manual intervention. The multiplexer-control-circuitry was built around a PIC16F871 microcontroller from Microchip. The RS-232 serial port on this microcontroller was used to communicate with LabVIEW using VISA-Serial protocol. For 3 bit lines/electrode, we needed 39 pins for 13 electrodes. Microcontrollers, DIP version in particular, do not have that many I/O pins. In our case, the F871 has a total of 33 pins, not all of which can be used. A series of 74139 chips were used to decode

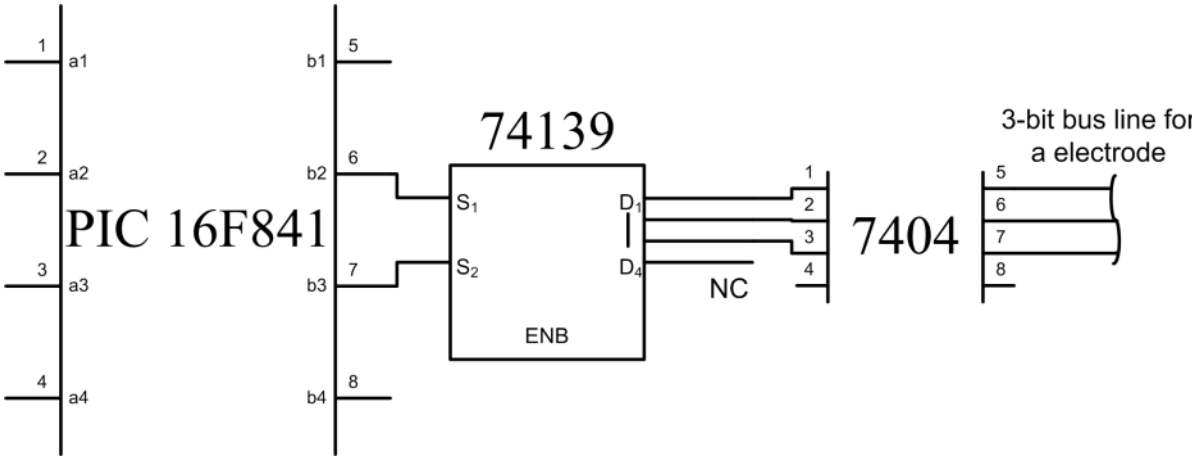

Fig 4-3 Decoding a 2-bit signal from the microcontroller to generate a 3-bit signal that is inverted to get active-high signal – PCB-A

2 I/O bits on the microcontroller to 3 bits at its output as shown in Fig 4-3. This reduced the required pin count from 39 to 26, which was affordable. However, provision was made for controlling 14 electrodes on the microcontroller, though the 14^{th} was not implemented on the multiplexer board. Since the decoder generated active low outputs, a series of 7404 chips were cascaded to invert the logic and "buffer" the opto-isolators that followed. The control logic described above was implemented on a PCB, denoted as PCB—A, with a RS-232 female header for interfacing with the computer, IDC connection headers which carried the control signal out, a 14.7456MHz SMD crystal that drove the micro-controller and the omnipresent 7805 regulator.

PCB-A was followed by PCB-B, a group of 5 UOB8 opto-isolator boards purchased from Industrologic, Inc, MO. These boards provided the necessary galvanic isolation between the circuit logic on PCB-A and the multiplexer's relays, as shown in Fig 4-4. The need for PCB-B is due to the noise introduced into the power rails by the inductance of the relays while switching. This noise interferes with the RS-232 communication of the microcontroller causing it to fail. The input resistor and opto-isolator were replaced with 1kohm and a H11B1 chip, respectively, to match the drive currents necessary for reliably switching the relay. The H11B1 has a GaAs LED optically coupled to the base of a silicon photo-darlington transistor. While the emitter of each of these transistors were connected to ground at the header itself, the collectors and one common V_{cc} terminal were grouped into two IDC cables. The pull-up resistors at 10kohm were left untouched since they can serve a purpose similar to fly-back diodes. In other words, they conduct current in the reverse direction while the transistor switches off, thereby increasing the life-time of the relays. Though these diodes do draw current when the transistor switches ON, they do not affect the relay switching.

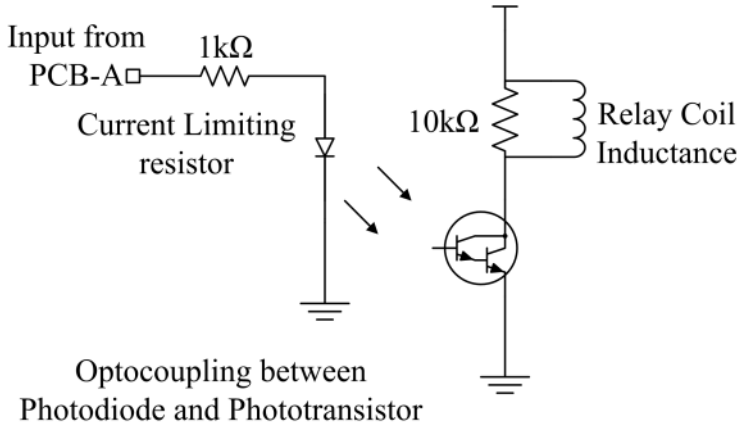

Fig 4-4 A schematic showing the input resistor exciting a photodiode which in turn switches on a phototransistor to cause current to flow through the relay coil inductance – PCB-B

An IDC cable connected the header output of PCB-B to the multiplexer board, PCB-C, described earlier. The program on the microcontroller performed the task of communicating with the computer over the serial port and setting the coded bits on the I/O ports. A device-address based instruction was defined to which the microcontroller responded. A valid instruction was responded with "OK" as an acknowledgement. Thus, in LabVIEW, an Automatic-Repeat-reQuest (ARQ) was implemented to ensure that the desired electrode was switched to the right configuration. The format currently used is "ALxxxxxxxxxxxxxx". The intial AL is fixed while the following 14 characters represent the state desired for 14 electrodes (only 13 have been implemented in PCB-C though). Each of those characters can take one of 4 values from 0 to 3 meaning Hp-Hc, GND, Lp-Lc pair and no connection in order.

This completes the measurement setup to measure the impedance of a multiple-site impedance sensor. A block diagram is shown in Fig 4-5.

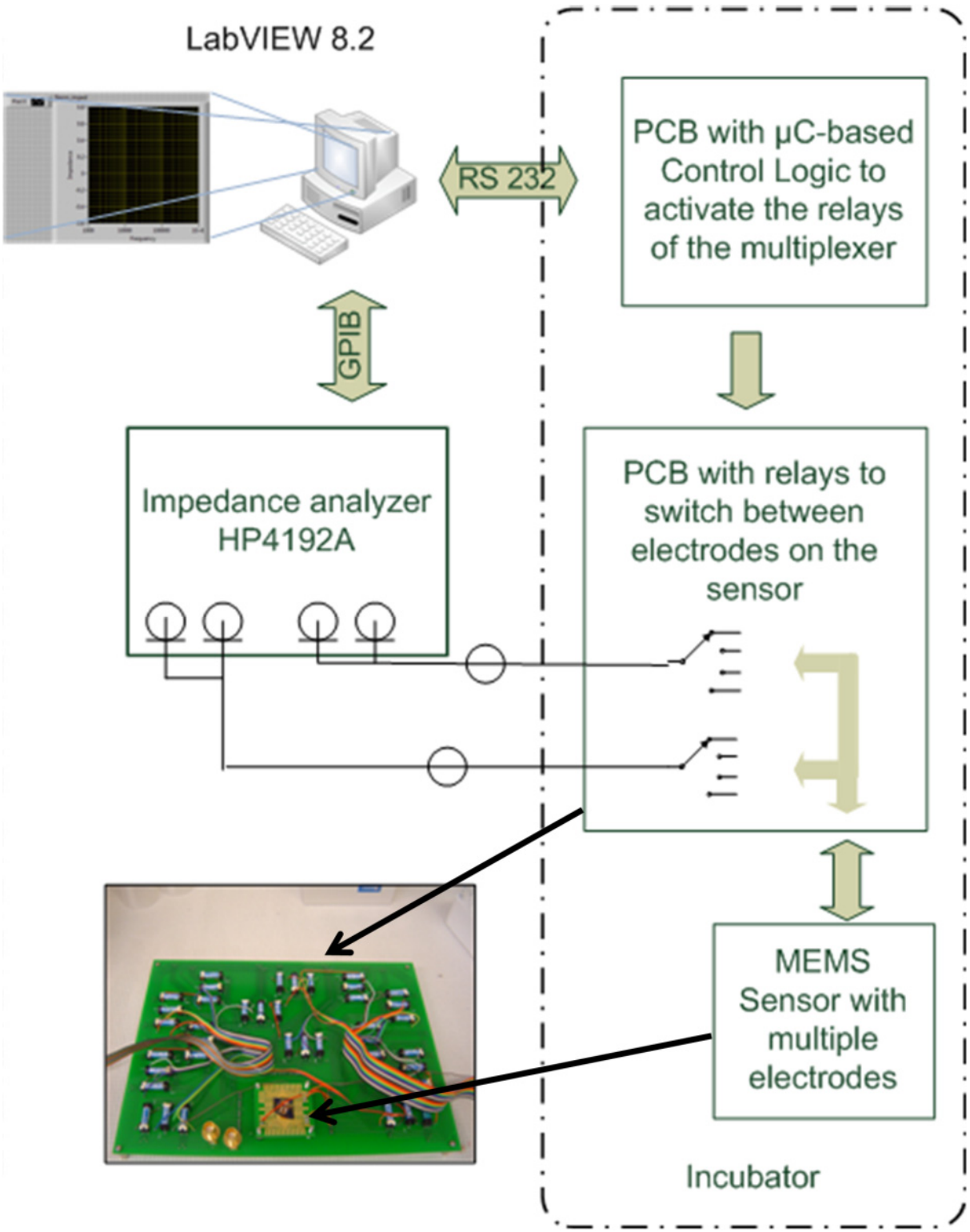

Fig 4-5 Automated measurement setup showing the connection between computer, impedance analyzer, multiplexer and the packaged sensor (to be explained in next chapter)

5 LAYOUT DESIGN AND FABRICATION

Bio-impedance chips with multiple sensing sites were designed. There are two generations of designs that will be reported in this document. The fabrication for both designs was a simple 2-mask process. A 500μm-thick 4-inch <100> single-side polished silicon wafer was the starting material in both cases.

5.1 Layout of First Generation Device

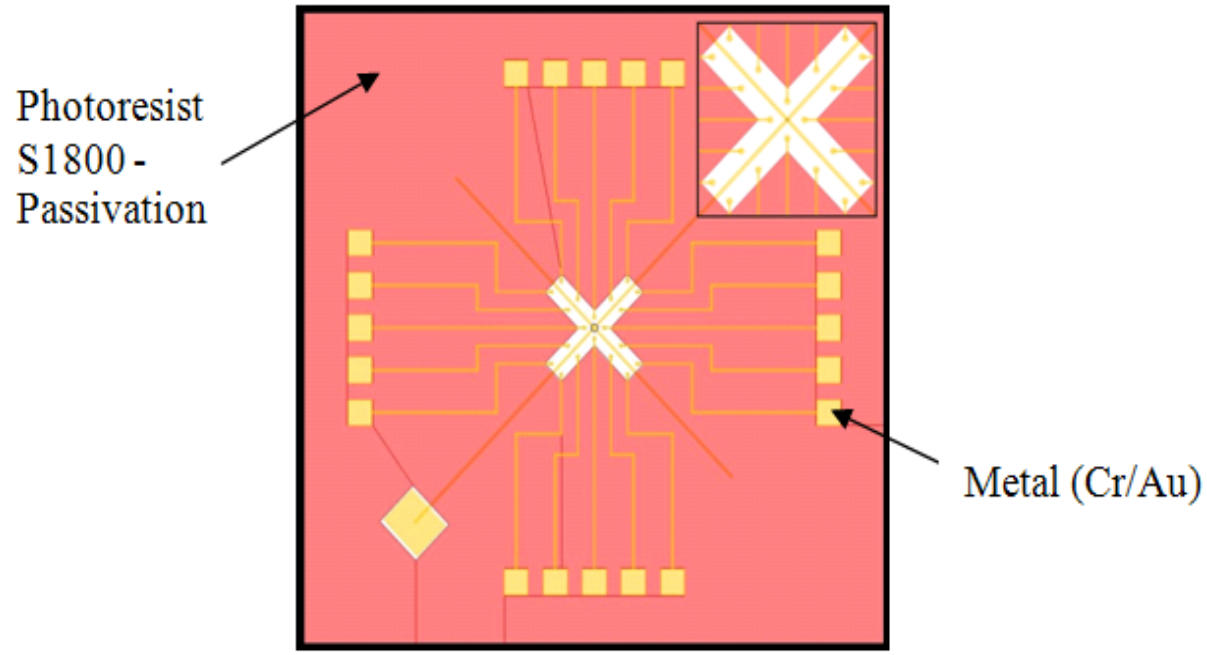

Fig 5-1 Layout of first generation device

A snapshot of the layout of first generation device is shown in Fig 5-1. This first generation chip was fabricated using a process flow that incorporated electroplating to achieve a comparatively larger thickness of electrodes. It was designed by Mr. Mehdi Nikkhah from VT MEMS Lab. This design is more application oriented.

There are multiple electrodes with the counter electrode passing symmetrically across the diagonal of the chip. Each individual electrode is 30µm wide and has a circular tip with 45µm in

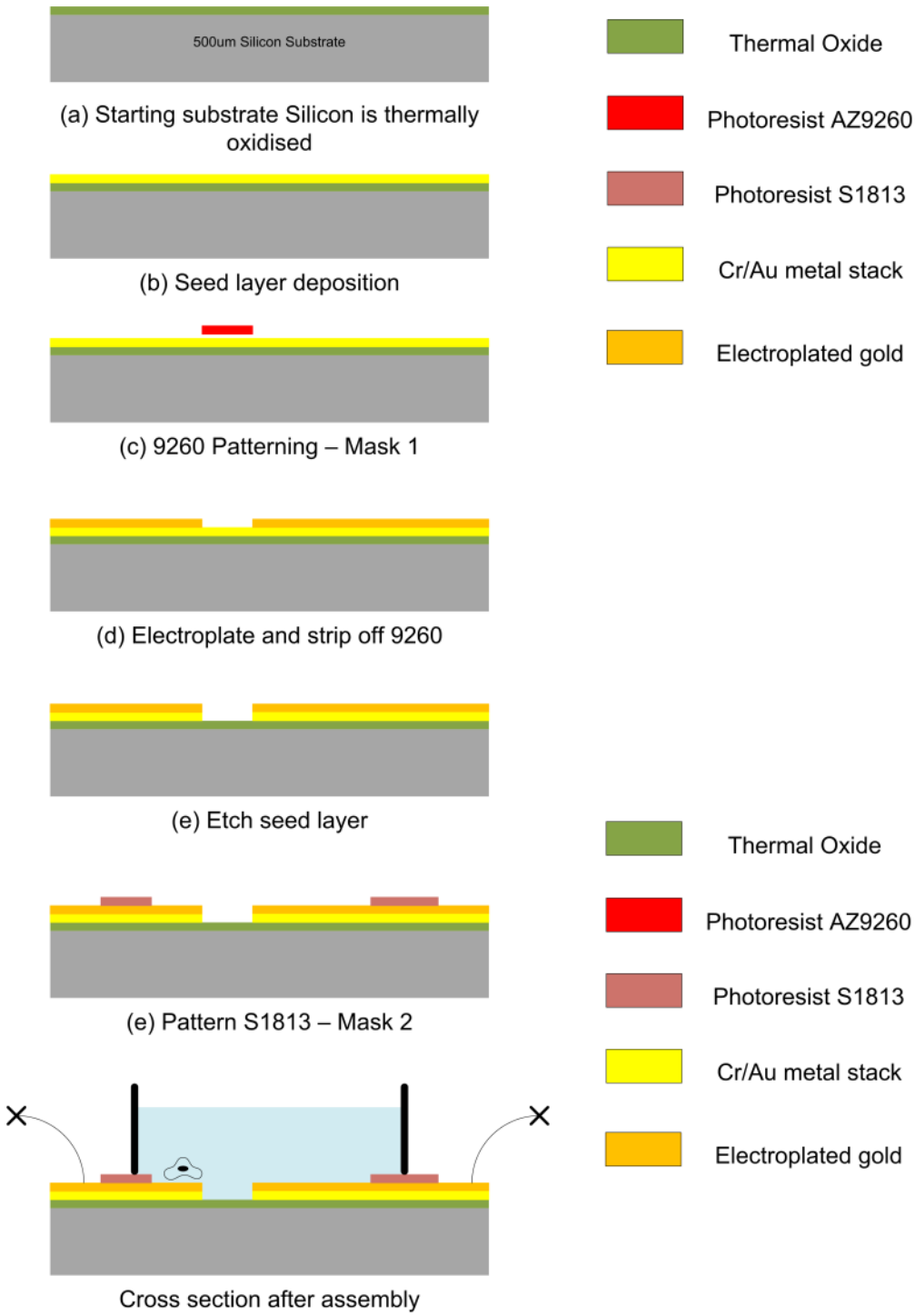

Fig 5-2 Fabrication process flow for first generation device

radius. There is a 500µm square bond pad to interface with each electrode. Fabrication, depicted in Fig 5-2, starts with oxidizing the silicon wafer to grow ~5000Å-thick oxide layer by thermal oxidation. This was followed by evaporation of 300Å/500Å Cr/Au to form the seed layer. A 6µm thick photoresist, AZ 9260, spun-coated onto this wafer was patterned using Mask 1. The Au layer that was exposed through the photoresist was electroplated to a thickness of ~2.5µm. The photoresist was stripped off and the Au and Cr seed layers etched back. The passivation layer was prepared by spin-coating a layer of S1813 onto the wafer and by patterning with Mask 2 to expose the bond pads and the sensing window.

The last figure shows the cross-section of the packaged sensor. The thick black lines correspond to the cloning cylinder which is fixed to the sensor using photoresist itself. This holds the medium in which cells are inoculated. Electrical connection to the bond pads were made by wire-bonding onto the traces on a PCB. The wires from the multiplexer were soldered onto vias on the traces of the PCB. A small strip of Parafilm was used to close the lid of the cloning cylinder and prevent evaporation of the medium.

5.2 Layout of Second Generation Device

I designed the layout for second generation device and this was geared more towards characterizing the measurements in terms of various parameters. Some features of the second layout are listed here:

a) The area of the electrode within the same design was varied to establish the relation between area and impedance measured.

b) The distance of the electrodes from the counter-electrode was varied to observe the difference, if any.

c) At the least, two electrodes of the same design parameters were used to ensure verification when impedance is measured.

d) Symmetry of the design was maintained such that each electrode faces the same environment as its duplicate in the same design.

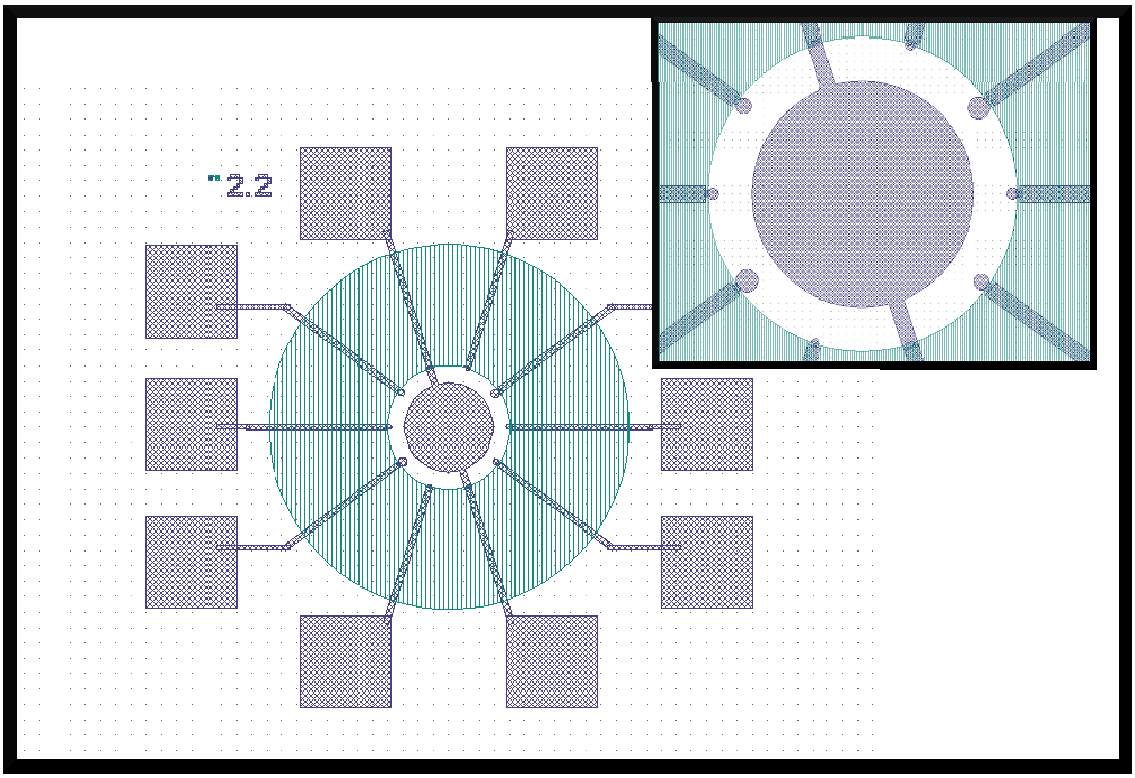

Fig 5-3 Layout of second generation device

A snapshot of the layout for the second generation device is shown in Fig 5-3. The counter electrode, the large circle at the center, is approximately 2900µm in diameter. The sensing electrodes are placed the same distance away from the counter electrode in the radial direction. There are 8 electrodes in all, two of each kind, placed diametrically apart. Thus, there are electrodes of 4 different areas corresponding to circular diameters of 100µm, 150µm, 200µm and 300µm. This structure provides a good symmetry for every electrode. Unlike the previous design, in this case, electroplating was avoided, since it seemed to have no effect.

The process starts with growing a thin layer of oxide, ~500nm, to serve as an insulation

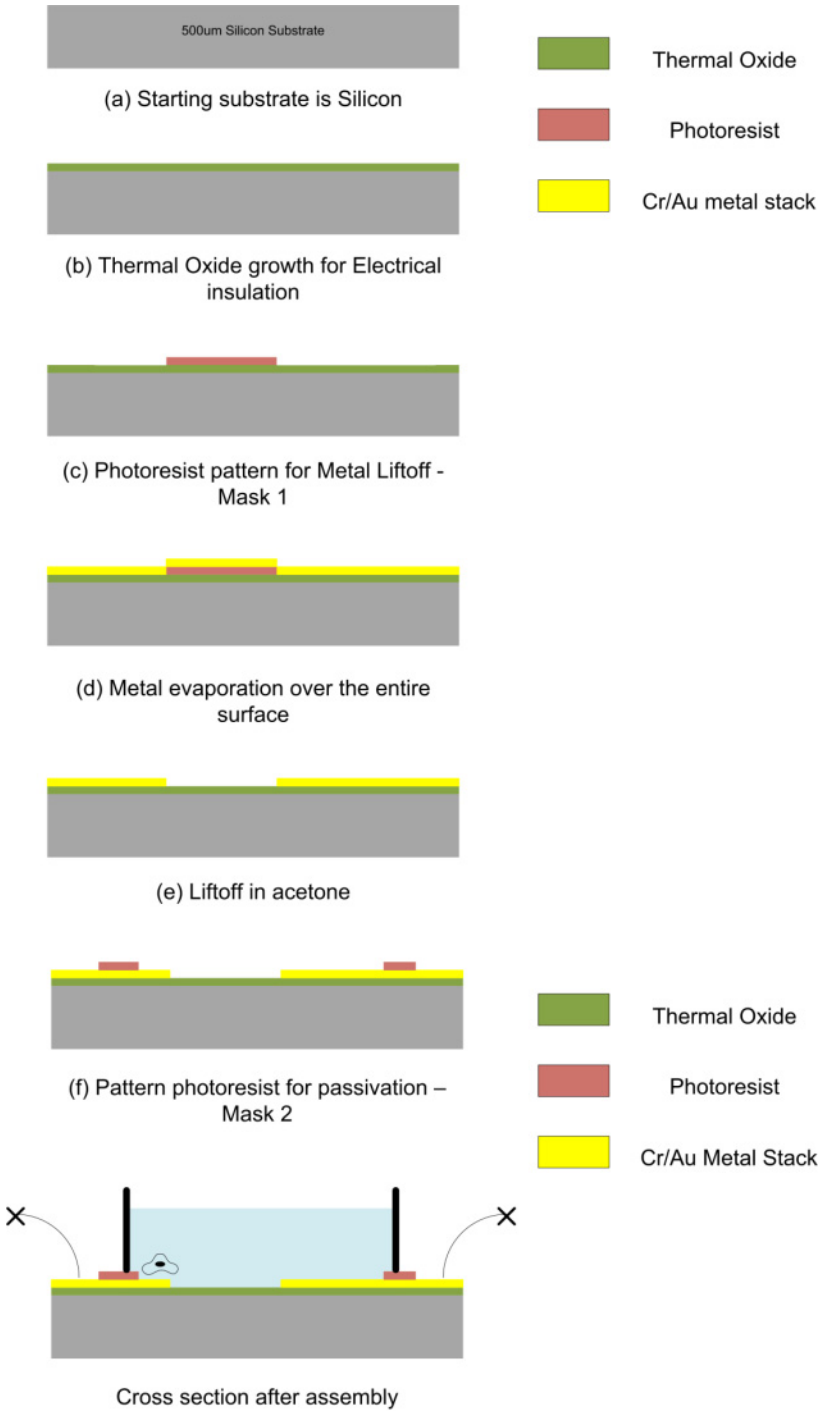

Fig 5-4 Fabrication process flow for second generation device

layer. Following this, a layer of photoresist S1827 was spun coated, at 4000rpm to a thickness of ~2µm. After a soft bake at 100˚C, the wafer was exposed using Mask 1 and then developed in

MF319. These developed wafers were mounted onto the platen in a KJL-PVD-250 e-beam evaporator. Chromium (for adhesion) and gold were evaporated to a thickness of 50nm and 150nm, respectively, in order in a single run.

The evaporated wafers were then immersed in acetone so that the photoresist along with the metal on top of it are removed. However, the metal which was directly in contact with the substrate is not removed. A small amount of sonication is necessary to remove the metal off. The final step was to prepare the passivation layer, by spin-coating photoresist. The area of the metal that is left exposed after this patterning step includes the area which is part of the sensing area as well as the area which is meant for electrical contact with the electrodes, i.e. bond pads.

The last figure shows the cross section of the packaged sensor. The electrical connections to the bond pads are achieved by soldering the wire from the multiplexer directly onto the pad. The pad in this case is approximately 3mm on each side and the interconnect width is ~200μm. The thick black lines represent the cloning cylinder which is stuck to the bottom by dipping it in photoresist. Unlike the previous case, the sensor is packaged within a culture-dish container. The lid serves to reduce the evaporation rate of the medium though simultaneously allowing exchange of gases, especially CO_2 with the surroundings.

5.3 Assembly for experiment

In this work, MDA-MB-231 human breast cancer cells were purchased from American type culture collections (ATCC). Cells were maintained in plastic T-75 cm^2 culture flasks in RPMI culture medium which contained 10% fetal bovine serum (FBS), 1 mM sodium pyruvate, and penicillin-streptomycin (100 Units/ml). Cells were grown for at 5.5% CO_2 at 37ºC. The experiment was done under the same conditions except that the cloning cylinder replaced the T-75 culture flasks.

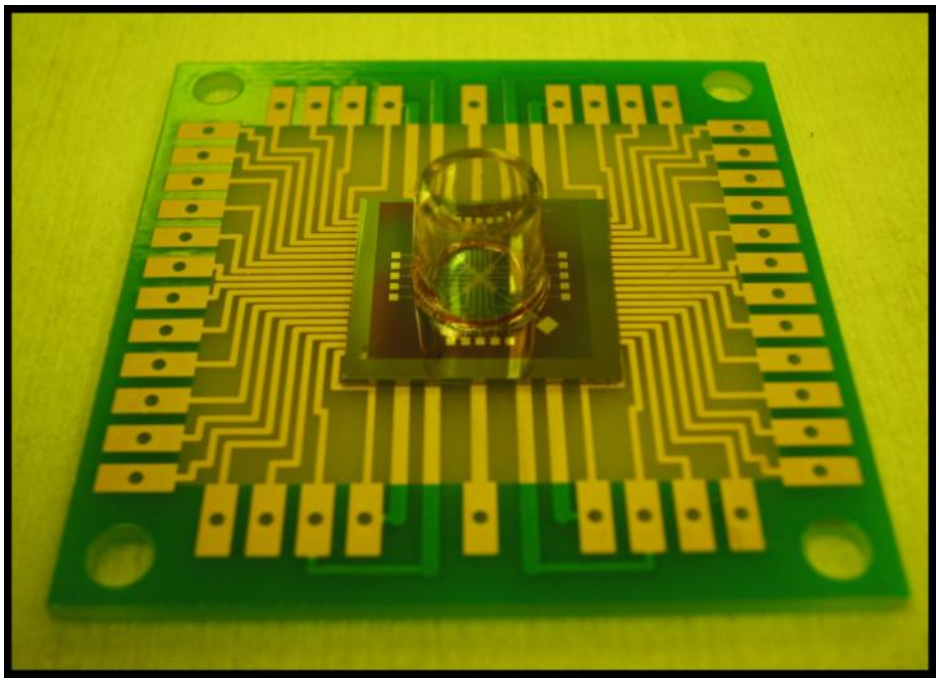

Fig 5-5 A assembled sensor on a PCB

The packaged sensor, in Fig 5-5, with electrical fixture was placed in the multiplexing board and the IDC header connected to the one that comes out of the multiplexing board, completing the setup and ready for an experiment.

6 EXPERIMENT, RESULTS & DISCUSSION

6.1 Cell-attachment to the sensor surface

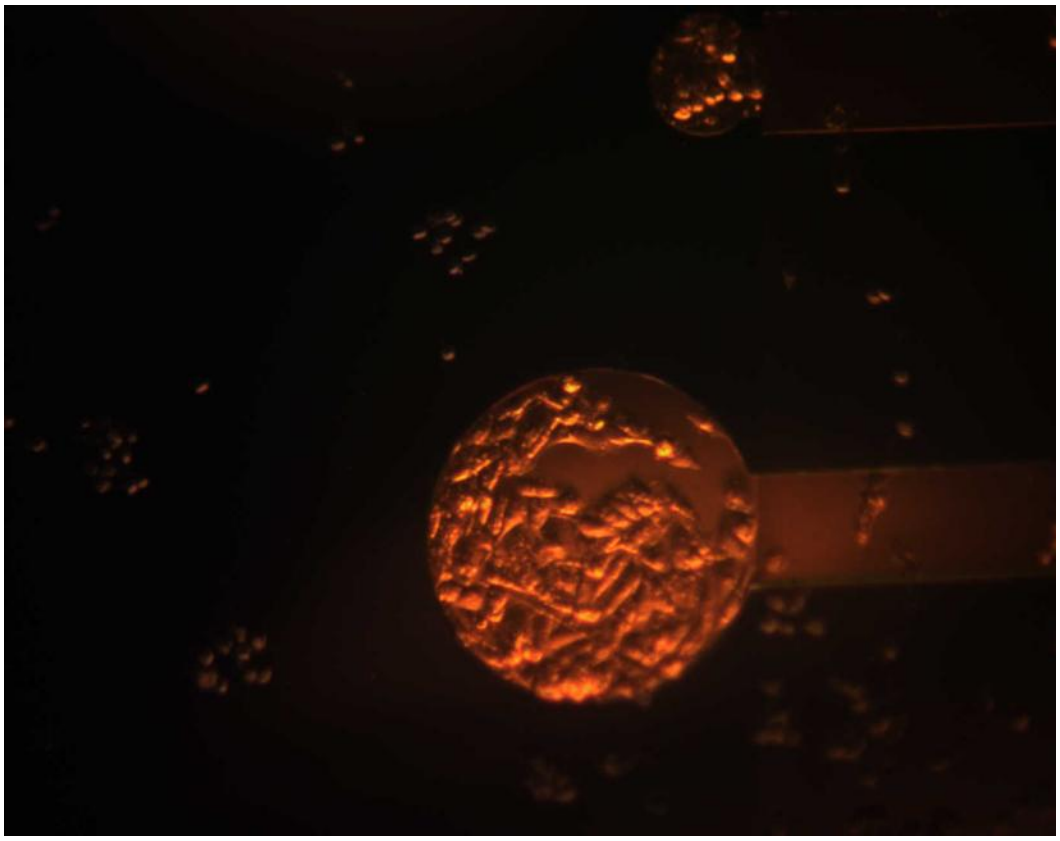

Fig 6-1 Optical image of cells on an electrode surface after 24 hours

An optical image of MDA-MB-231 cells cells on the same electrode of a sensor, 24 hours and 48 hours after culturing, are shown in Fig 6-1 and Fig 6-2. The cells are observed to crowd on gold rather than silicon dioxide. Cell membranes consist of various molecules which comprise of carboxylic groups (–COOH). These dissociate in an electrolyte to form negatively charged – COO^- groups. This causes cell membranes to be negatively charged[48]. Silicon dioxide (Point of Zero Charge (pH) - 2), is negatively charged or a cation adsorber in the culture medium (pH

~7.2). Finally, gold, is an inert material. Hence, it is possible that cells prefer to attach onto gold rather than silicon dioxide, if provided with an option.

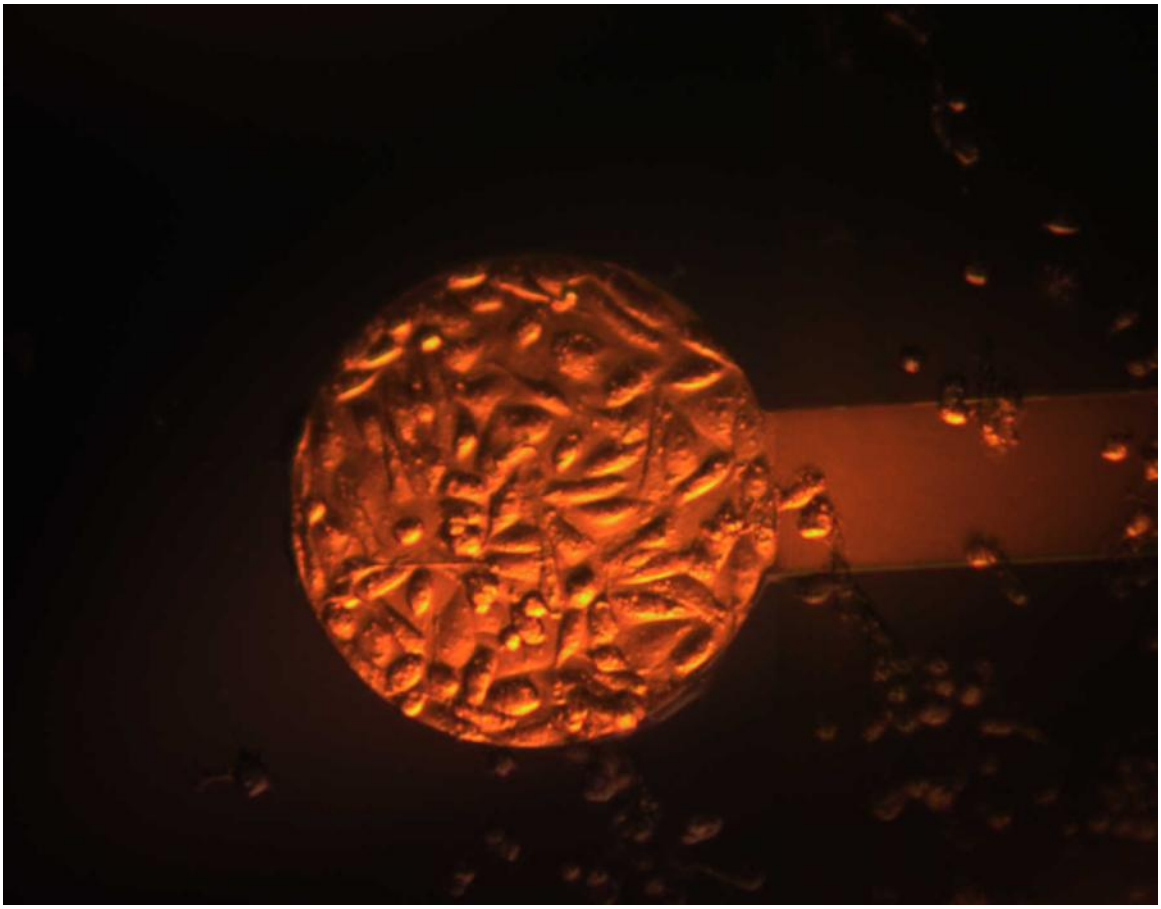

Fig 6-2 Optical image of the cells on the electrode surface after 48 hours

Another possible parameter that was analyzed for any possible role in the attachment of MDA-MB-231 cells to the surface was stiffness of the surface itself. The reported values for the elasticity of gold and thermally grown silicon dioxide are 69 GPa and 72 GPa, respectively [49, 50]. Since these values are not significantly different, this may not be the reason for the preferential attachment. Also, cell attachment studies made on separate silicon dioxide and gold surfaces (data not shown here) did not reveal any significant difference. In short, cells prefer

gold over silicon dioxide when given a choice likely due to different polarity in surface charge. These results, however, are not conclusive and need further investigation.

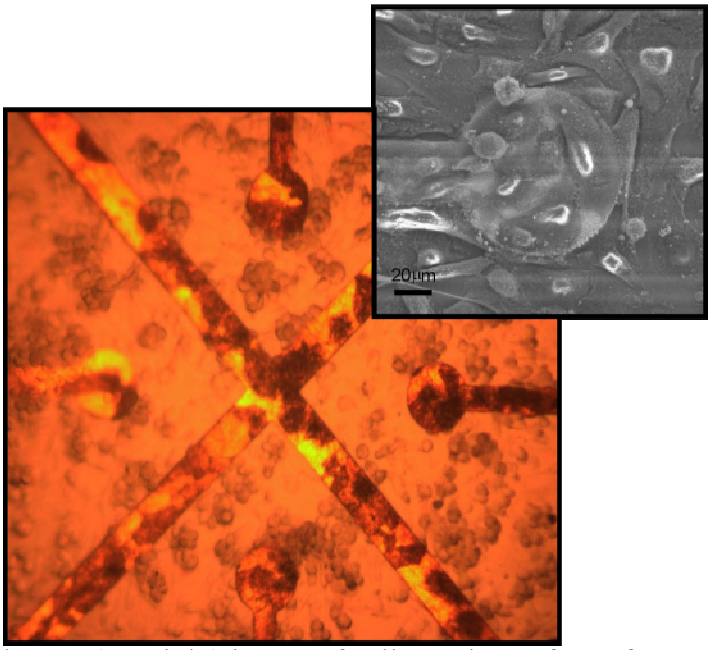

Fig 6-3 Optical and SEM (top right) image of cells on the surface of second generation device

Fig 6-3 shows the cells grown on the surface of Design 2 sensor. The initial seeding density was high and hence a large number of cells can be seen. The image on the top right is the SEM image of the fixed cells after 24 hours of culture.

6.2 Impedance of medium

Fig 6-4 plots the impedance of medium on electrodes of effective diameter 300µm and 100µm in Design 1. These measurements are successive runs on the same electrode. The excitation voltage was 50mV and the frequency swept from 1 kHz to 1 MHz at 10 points per decade. The impedance for the 300µm electrode is capacitive in the low frequency range, flattens out in the moderate frequency range around 100kHz, and then slopes capacitively towards the right extreme. The components that contribute to this response are C_{dl}, R_{sp} and C_{par} in order. Z_p is

ignored for this modeling. Since, the impedance of C_{dl} is inversely proportional and in series with R_{sp}, for the smaller electrode, the moderate frequency flattening is not observable in the magnitude plot. However, the phase plot is more sensitive to the variations.

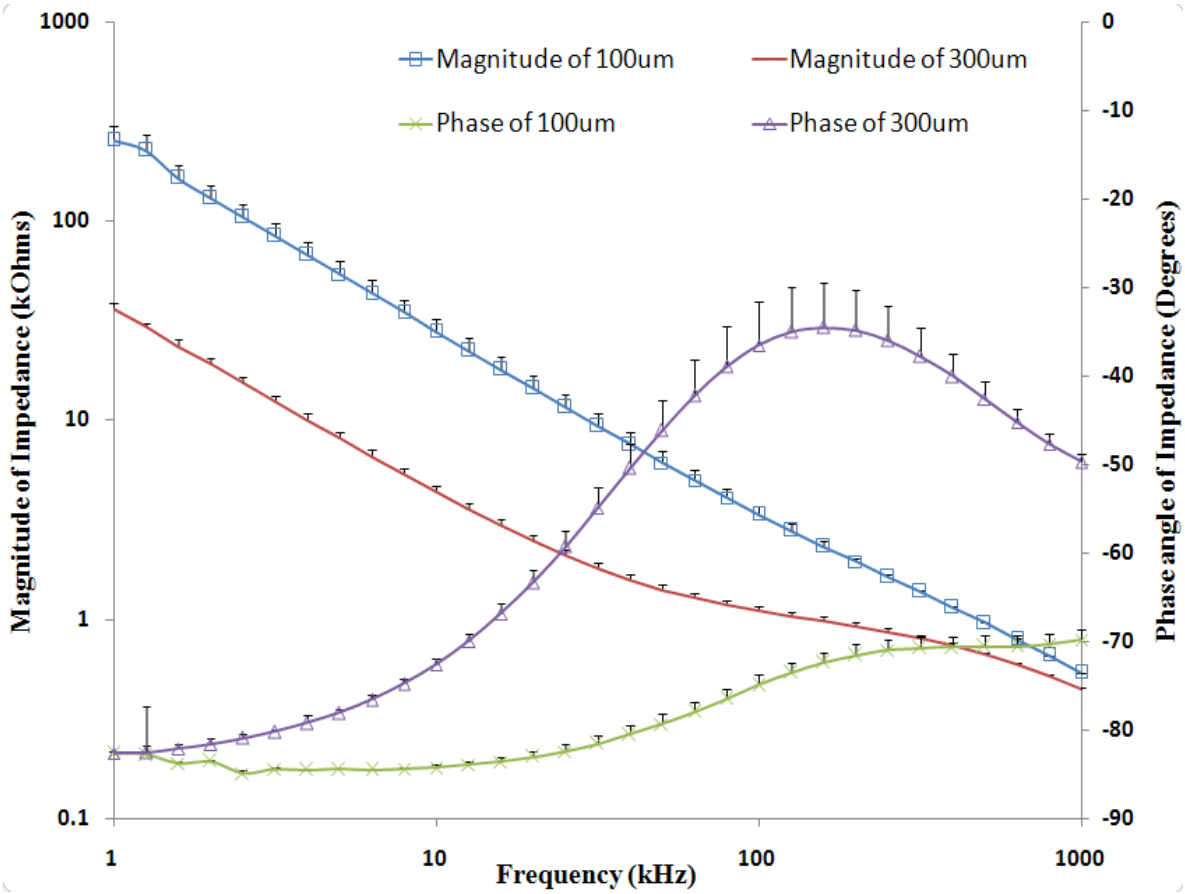

Fig 6-4 Impedance plots of electrodes of area 100µm and 300µm

Measurements were made on the same electrode for different voltages to determine the signal to noise ratio. It was observed that with decreasing voltage, the low frequency measurement was minimized in range and noisier (data not shown). However, the voltage cannot be arbitrarily increased, since it is possible to cause physical damage to the cell membrane, reversible and irreversible [21].

The simulated magnitude of the impedance of 300µm electrode without cells along with the relatively weighted error at each frequency is shown. Overall, the error was 0.0078. The

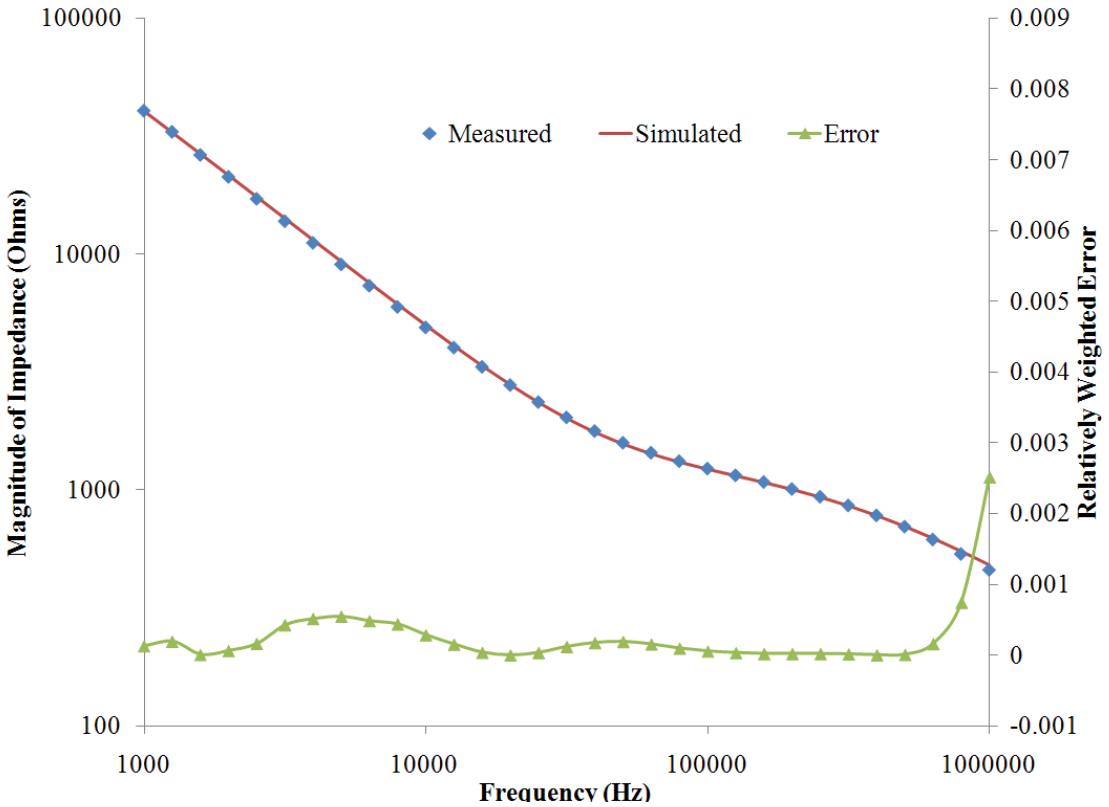

Fig 6-5 Simulated magnitude of the impedance of a 300µm electrode compared with the measured value.

parameters for the simulated plot are not optimal. The phase angle of the impedance has been simultaneously fitted and the plot along with the relatively weighted error is shown in Fig 6-6. The overall error in the phase plot is 0.00475. The parameters obtained in this fitting are listed in Table 6.1. C_{dl} and C_{par} are modeled as Constant Phase Elements (CPEs) while R_{sp} is an ideal linear resistor.

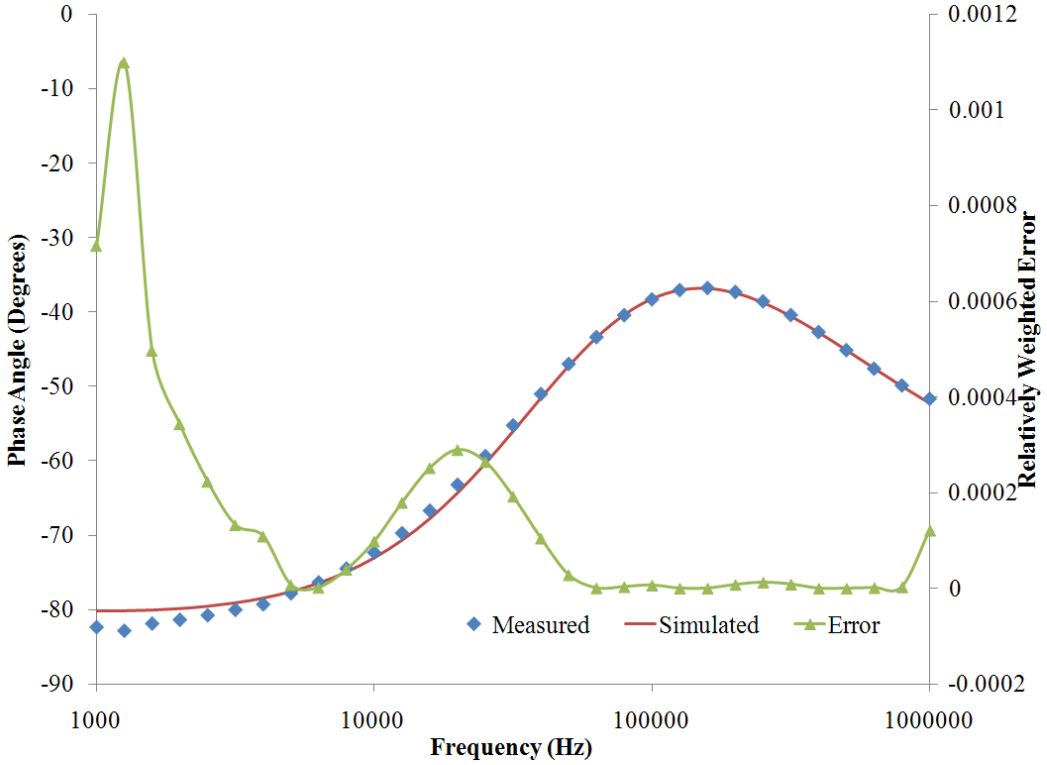

Fig 6-6 Plot of the measured and simulated values of the phase of the impedance of the medium along with the relatively weighted error.

Circuit Element	Parameter : Value
C_{dl}	C_{coeff} : 2.9e-4, n : 0.98
R_{sp}	$R_{spcoeff}$: 4.2e-1
C_{par}	$C_{parcoeff}$: 3.7e-11, n_{par} : 0.76

Table 6-1 Parameters and values obtained by fitting the impedance of the medium

6.3 *Impedance of the electrode with cells*

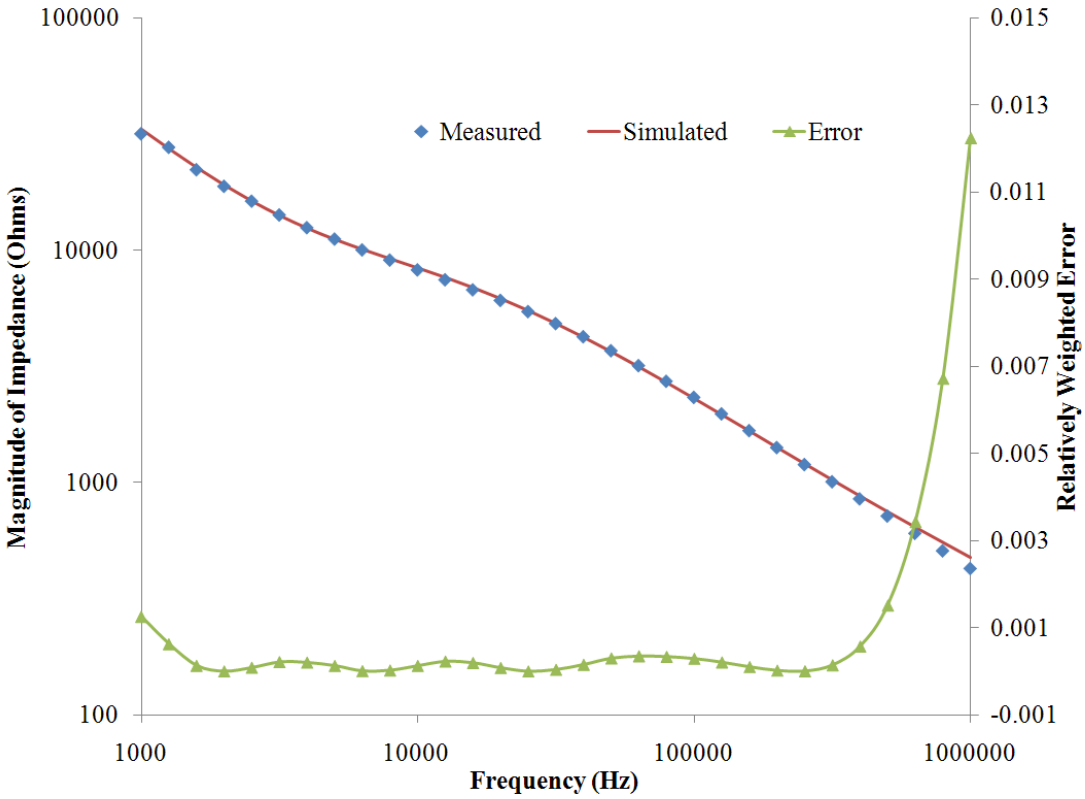

Fig 6-7 Measured and Simulated magnitude of the impedance of the electrode in the presence of cells after 24 hours of culturing.

Fig 6-7 and Fig 6-8 are plots of the measured and simulated values of the impedance of the electrode 24 hours after culturing cells on it. For this simulation, the values of the parameters except for the RC model of the cell were obtained from the previous section. However, it should be noted that in the presence of cells, the low frequency impedance drops and this has been attributed to adsorption of protein generated by cell metabolism[27]. Hence, a scaling factor of 1.4 has been included for the double layer capacitance, $C_{dlcoeff}$. The capacitance in the RC model is a CPE, and is proportional to the area of the electrode while the resistance is inversely proportional to the area of the electrode.

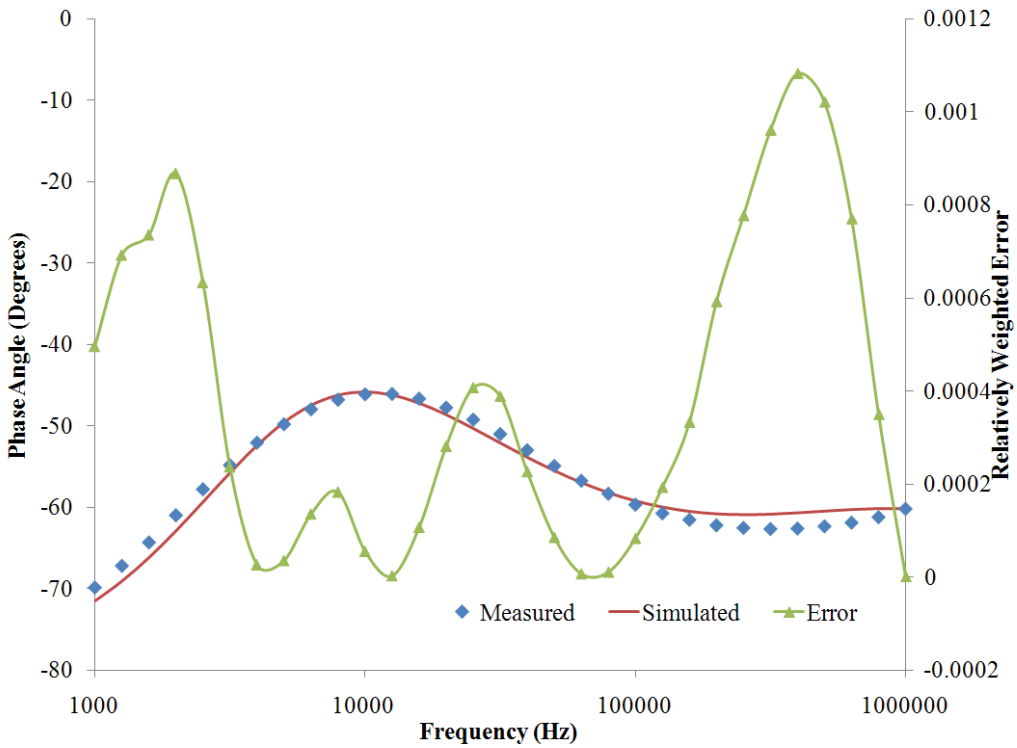

Fig 6-8 Simulated and Measured values of the phase of the impedance of the electrodes in the presence of cells culture for 24 hours

The parameters and the values obtained are listed in Table 6-2.

Circuit Element	Parameter : Value
R_{gap}	7.8e-4
C_{cell}	$C_{cellcoeff}$: 0.52e-3, m : 0.83

Table 6-2 Parameters extracted from the impedance measured in the presence of cells

The normalized impedance is plotted in Fig 6-9 since the change in the impedance is relatively insignificant to be observed in the log-log absolute plots. The normalized plot is defined in Eq 6.1, where the '[]' indicates the absolute magnitude of the complex quantity

$$\Gamma = \frac{[Z_c] - [Z_m]}{[Z_m]} \tag{6.1}$$

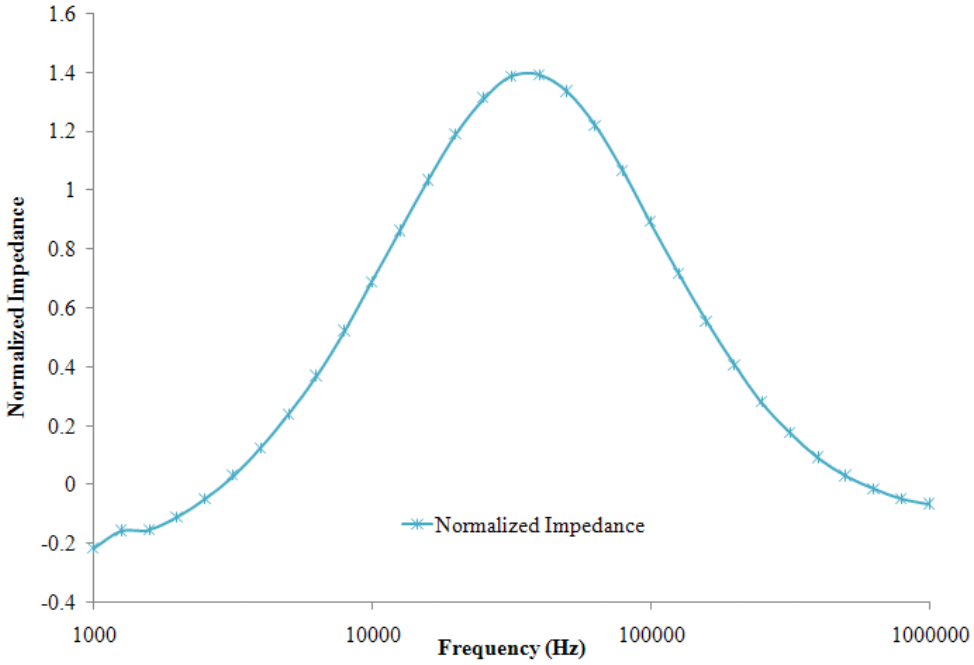

Fig 6-9 Normalized Impedance of the impedance of the electrode 24 hours after culturing cells against the impedance without the cells

The increase in the impedance can be explained based on the manner in which cells attach to a surface. Cells are in contact with the surface of a substrate only for an area <6μm^2 while the rest is separated from the substrate by a distance[25]. This small gap gives rise to a resistance that is modeled as R_{gap}. C_{cell} is a combination of the cell membrane capacitance, solution resistance of any uncovered area on the electrode. As a cell comes in contact with a surface, it attaches and spreads out. The cell-surface gap reduces, increasing R_{gap} and in turn increasing the measured impedance. This is seen as an increasing curve in the normalized

impedance. However, beyond a certain point it is dominated by C_{cell} at which point the curve peaks and begins to drop resulting in the measured profile.

6.4 Time Evolution of Normalized Impedance Peak

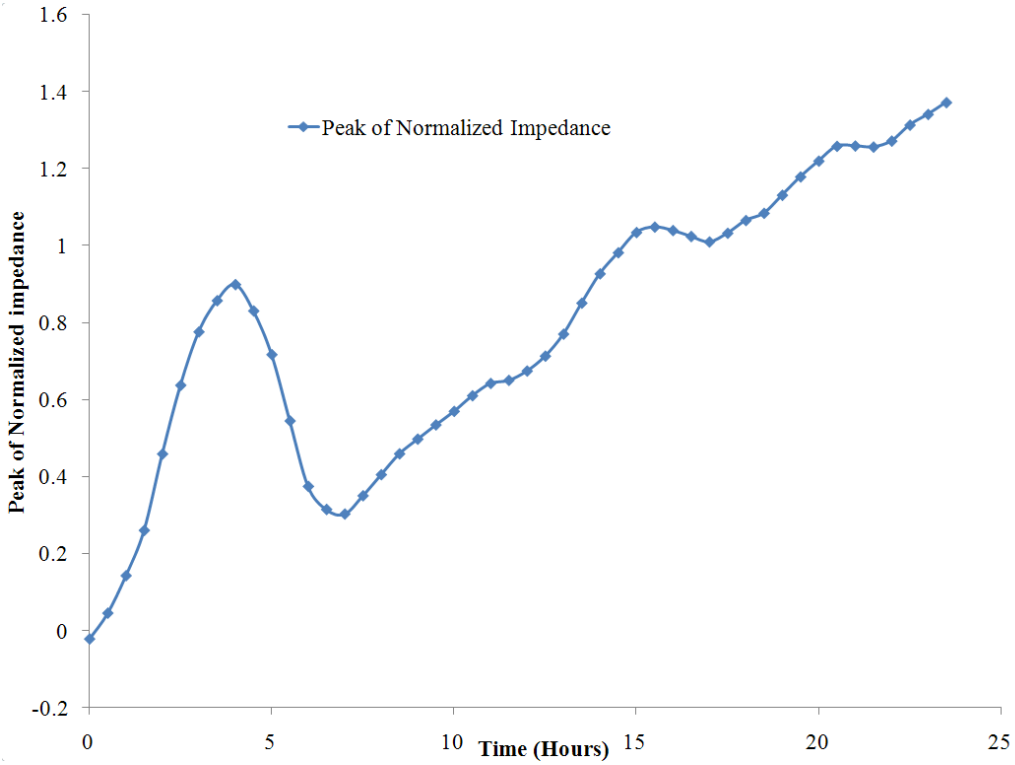

Fig 6-10 A plot of the peak of normalized impedance on the same electrode analyzed above over a period of 24 hours. The dip around 4 hours should correspond to detachment of cells as medium started evaporating. However, medium was refilled and covered with a Parafilm after which the value began increasing gradually.

From the explanation in the previous section, it can be inferred that a time evolution of the peak of the normalized impedance is increasing until it attaches. Fig 6-10 shows the time evolution of the same electrode that was analyzed above. The data has been smoothened using a 4 point average, i.e. y[n] = (x[n] + x[n-1] + x[n-2] + x[n-3])/4. After the experiment was started, it was observed that the medium was evaporating over time due to non-air-tight lid. This seemed

to have caused the cells to begin detaching on a few electrodes. This behavior was noticed in a previous experiment in which the medium had evaporated. However, this time around, medium was added around 4 hours and the peak was found to flatten and then increased indicating that the cells had begun attaching again. The peak is supposed to saturate once the cells attach to the substrate until it detaches once again for cell division. It can be concluded that cells were piling onto the electrode even until 24 hours. Due to lack of simultaneous video-recording, this behavior cannot be cross-checked as of now.

6.5 Experiment and Analysis of Passivation Layer

The passivation layer, in a bio-impedance sensor, serves to isolate the metallic interconnect lines, which connect the sensing sites to the bond pads outside the cloning cylinder, from the culture medium and cells above it. In the past, research groups used red wax, cover glass, epoxy etc[12, 27]. Photoresist was used in this research, since it can be integrated into micro-fabrication procedure and hence can reduce the cost. In this sub-section, the ability of the first-generation chip to monitor the growth of cancer cells over time and the effect of the non-ideality of the passivation layer in the sensor response is presented[51]. To achieve these objectives, two different scenarios are considered.

In Case I, the chip was placed within the incubator. The cloning cylinder was filled with 200µl of culture medium and a measurement across multiple electrodes was made from 1kHz to 1MHz. The impedance thus obtained is Z_{m1}, where the subscript ‘m’ denotes medium without cells and ‘1’ denotes case I. It should be noted that the parameters which contribute to this impedance are C_{dl}, R_{sp}, Z_{p1} (Z_{w1} and C_{p1}), and C_{par} as shown in Fig. 3.9. The culture medium in the cloning cylinder was then replaced by 200µl of the same culture medium containing MDA-

MB-231 metastatic human breast cancer cells. A high initial cell seeding density of $2x10^5$ cells/200µl was used. With the sensor exposed to the cells, a frequency sweep was performed once every half an hour for 24 hours and the impedance (Z_{c1}) data stored separately. The subscript 'c' indicates that the measurement was made after cells are introduced into the sensor. While there is only one data set corresponding to Z_{m1}, Z_{c1} has a measurement every half an hour and provides the response to the time varying adhesion of cells to the sensor surface. Z_{c1} is modeled similar to Z_{m1} except for the addition of Z_{cell} in the equivalent circuit.

The presence of cells will increase the impedance measured. However, this increase is relatively small in the plot of the absolute impedance. This change will be more clearly noticeable if the impedance in the presence of the cells is normalized with respect to the impedance in the absence of cells; i.e., the culture medium, given in Eq. 6.2. Referring to Fig 3-4, in Case I, Γ_1 can be rewritten as

$$\Gamma_1 = \frac{([Z_{sc1}] \,||\, [Z_{pc1}]) - ([Z_{sm1}] \,||\, [Z_{pm1}])}{([Z_{sm1}] \,||\, [Z_{pm1}])} \tag{6.2}$$

where, the subscripts 's' and 'p' corresponds to sensing window and passivated area, respectively. The parasitic component has not been shown though it is used in calculations. The actual normalized impedance when having an ideal passivation layer (i.e., with Z_p equal to infinity) is given by:

$$\Gamma_{actual} = \frac{[Z_{sc1}] - [Z_{sm1}]}{[Z_{sm1}]} \tag{6.3}$$

In Case II, the chip surface including the sensing window was completely covered with photoresist and hence passivated. As in the previous case, the cloning cylinder was filled with the culture medium and a measurement was made (Z_{m2}). Since there is no sensing window in this case, the impedance measured consists of only the Z_p branch, albeit with the modified component values C_{p2} and Z_{w2} which differ from C_{p1} and Z_{w1} because of the slight differences in area of the passivated region in the two cases. The medium was then replaced by one with cells and the impedance measured once every half an hour (Z_{c2}). Z_{c2} includes a contribution from the cells which adhere onto the passivation layer. Since, we are using a high cell seeding density we can assume similar conditions in the biological environment with respect to Case I and II.

C_{p2} and Z_{w2} are proportional to the area of the passivated region raised to an exponent between 1 and -0.5, respectively. Therefore, we can write:

$$C_{p2} = \left({A_2}/{A_1}\right)^{1} * C_{p1} \tag{6.4}$$

$$Z_{w2} = \left({A_2}/{A_1}\right)^{-0.5} * Z_{w1} \tag{6.5}$$

By design, the area of the sensing window of the chips presented herein (A_1) is 10% of the entire sensor surface (A_2). Thus,

$$\frac{Z_{p2}}{Z_{p1}} = \frac{C_{p2} || Z_{w2}}{C_{p1} || Z_{w2}} = 1.1 \tag{6.6}$$

Using Eq. 6.6 and by measuring Z_{m2} and Z_{c2}, we then have:

$$Z_{pm1} = \frac{Z_{pm2}}{1.1} = \frac{Z_{m2}}{1.1} \tag{6.7}$$

$$Z_{pc1} = \frac{Z_{pc2}}{1.1} = \frac{Z_{c2}}{1.1}$$

Having known these two values and by measuring Z_{m1} and Z_{c1} in Case I, we can determine the impedance of the Z_s branch alone in Case I and obtain Γ_{actual}. This procedure can be applied to measurements taken from each individual electrode or to the average of all measured impedances at each time interval. It is noteworthy that we have analyzed only 13 of the 20 sensing electrodes due to the limitations on the multiplexer implemented. We have taken the average of the 13 electrodes to study and analyze the results.

Fig 6-12(a) shows the plot of the impedance measured in Case I in the absence of cells (culture medium) and that measured 24 hours after cells have been introduced; i.e., Z_{m1} and Z_{c1}. There is a drop in the impedance at low frequencies which has been attributed to the proteins accumulating on the surface due to cell metabolism [15]. Fig 6-12(b) is a plot of the impedance measured in Case II; i.e., Z_{m2} and Z_{c2}. Since, the impedance in this case is very high due to the absence of sensing window, especially at low frequencies, we can observe measurement noise which will manifest itself as sharp noisy peaks in the normalized plot. It is important to note that for an ideal passivation layer, we should not observe any change in the impedance regardless of the cell growth time.

A 24 hour plot of the normalized impedances after cells have been introduced has been shown in Fig 6-13 for Case I and Case II (i.e., Γ_1 and Γ_2). Fig 6-13(a) shows a peak at ~100 kHz which corresponds to the adhesion of the cells onto the electrode and it increases with time indicating the decreasing separation between the cells and the metal electrode. The amplitude of this peak saturates around 0.8 within 5 hours from introducing the cells to the sensor. In Fig

6-13(b) no peak is observed as there is a dielectric layer separating the cells and the metal electrodes. However, the cells affect the measured impedance which increases over time and saturates around 0.1 within the same time duration of 5 hours from cell addition to the sensor.

Using the measured results and following the aforementioned procedure Γ_1 and Γ_{actual} are derived and shown in Fig 6-11. Γ_{actual} is larger than Γ_1 indicating that the presence of the passivation layer and the cells that adhered on it can significantly lower the sensitivity of the

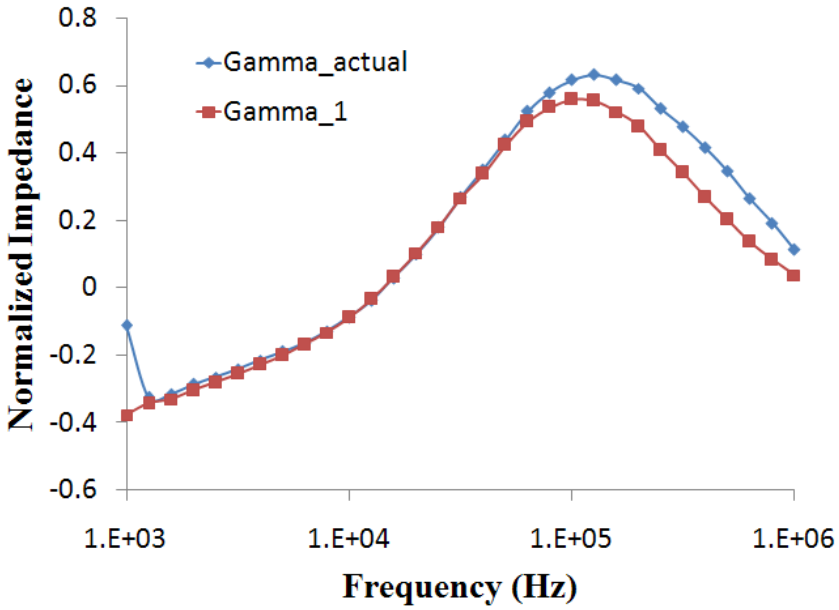

Fig 6-11 Γ_1 and Γ_{actual} have been plotted for the impedance measured after 24 hours. While the former is the measured value, the latter is the processed version of the measured value.

sensor to cells in the sensing window. This difference is observed to be negligible at low frequencies, increases at moderate frequencies (10kHz ~ 500kHz), and drops slightly at the upper end of the spectrum. The maximum drop in the response was determined to be 13%.

The significance of 13% can be observed in Fig 6-13(a) in which the difference between the 2 hour and 5 hour normalized impedance value is approximately 14%. What this means is

that, with an ideal passivation layer, where there is no drop of 13%, a 2 hour data would have had enough information as the 5 hour data. Also, the non-linear variation calls for a smaller electrode whose impedance will be dominated by the interfacial impedance and not the spreading resistance, resulting in Z_s and Z_p varying following the same capacitive trend.

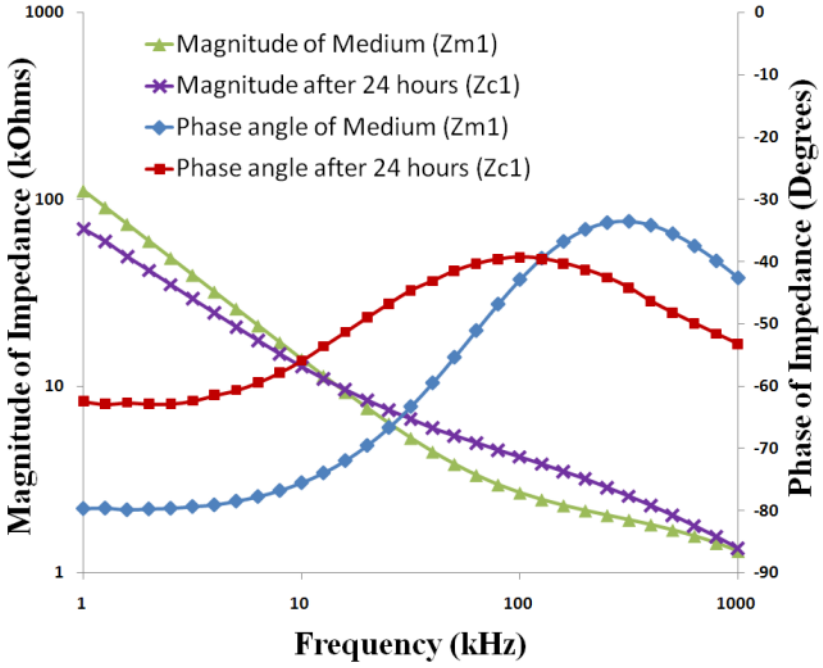

(a)

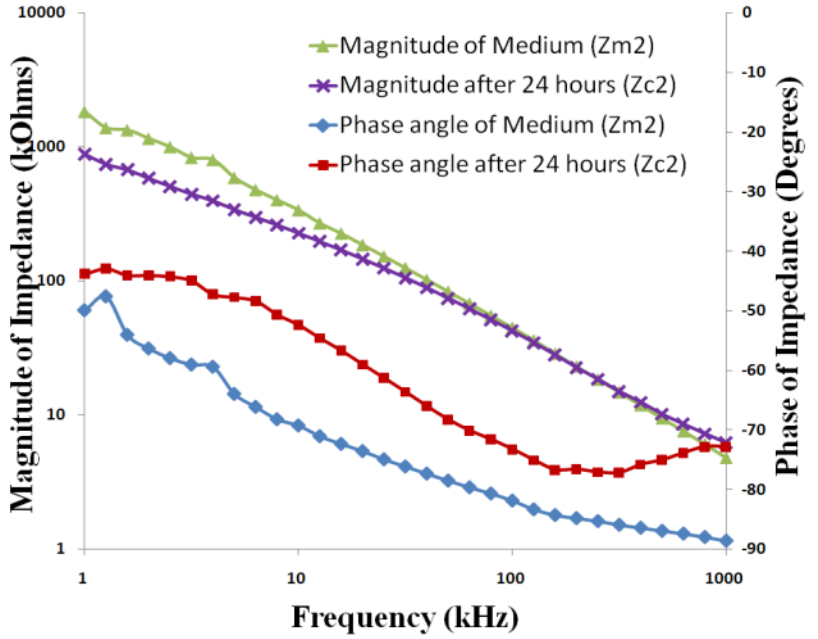

(b)

Fig 6-12 (a)Magnitude and (b) phase angle of impedance measured in Case I and II in the absence and presence of cells i.e. Z_m and Z_c

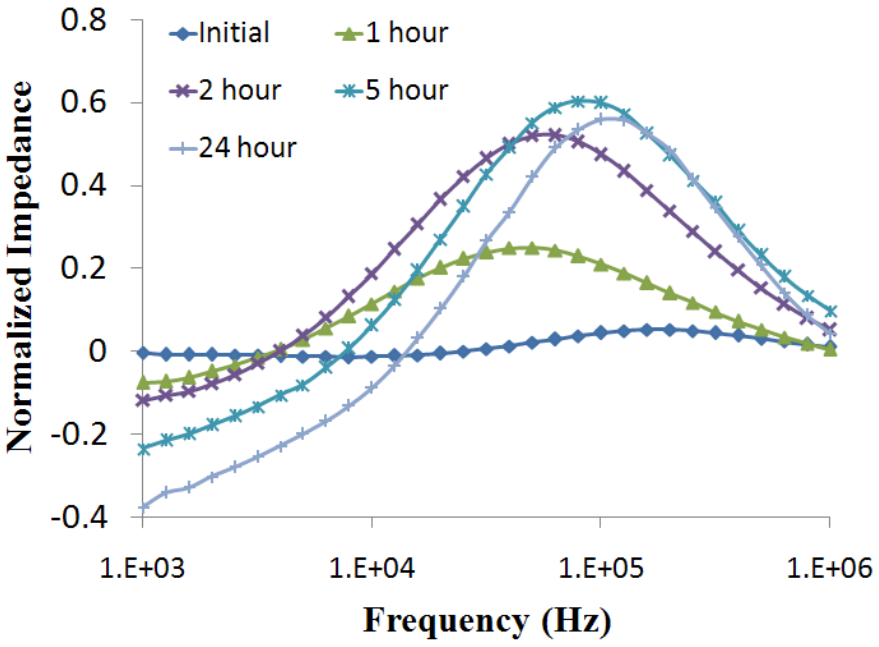

(a)

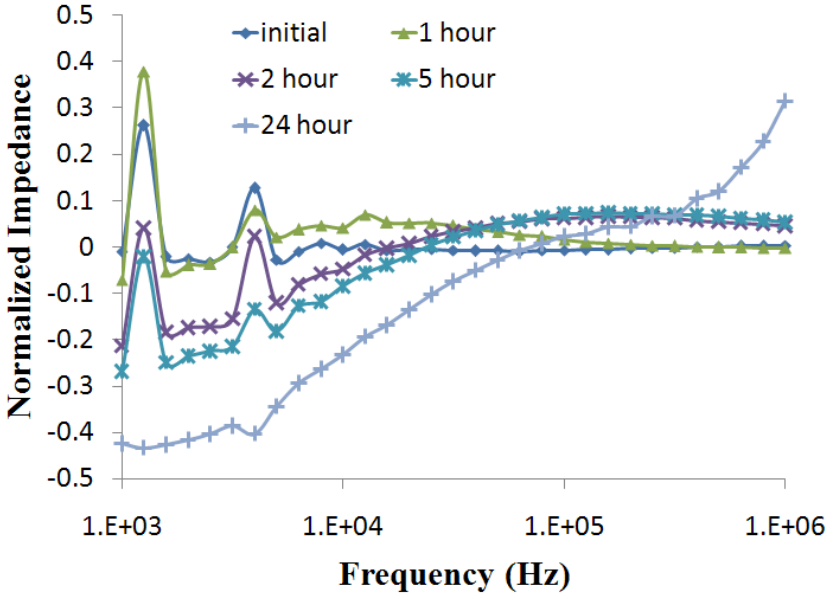

(b)

Fig 6-13 (a) and (b) show the 24 hour variation of the normalized impedance Γ_1 and Γ_2 for Case I and Case II respectively. Amplitudes saturate to 0.5 and 0.1 within 5 hours from the addition of cells in both the cases.

No.	Measurement Used	Parameter Extracted
1	Z_{m2}	C_p and Z_w are determined as CPEs – Z_{p2}
2	-	Z_{p1} is known from Z_{p2} using (6)
3	Z_{m1}	C_{par} as a CPE from the upper end of the spectrum
4	-	C_{dl} and R_{sp} as CPE and Resistor
5	Z_{c1}	Z_{cell} as a parallel RC circuit for measurement made after 24 hours

Table 6-3 List of measurements and the parameters extracted from the same

Parameter extraction was performed by manual inspection (trial and error) and the circuit model simulated for impedance plots using MATLAB. The measured impedances in this experiment are constant phase elements (CPEs) instead of an ideal capacitor, wherein the phase angle is not -90 degrees [27]. A CPE is characterized by an exponent 'n' and a coefficient 'C_{coeff}' such that its impedance is given by $1/(jwC_{coeff})^n$. This exponent manifests as the slope in the magnitude plot and constant phase in the phase plot. These two quantities are compared with the plot and the values of 'C' and 'n' determined. The parameter extraction procedure is tabulated in Table 6-3 and the parameters listed in Table 6-4.

Parameter	Impedance = $1/(j\omega C_{coeff})^n$
C_{dl}	Without cells: coeff = $4.5*10^{-10}$, n = 0.92 With cells: coeff = $1.25*10^{-10}$, n = 0.80
R_{sp}	$2.3*10^3$ Ω
Z_{cell}	C_{cell} : coeff = $6.7*10^{-11}$, n = 0.92; R_{cell} = $2*10^3$ Ω
C_{far}	coeff = $5.4*10^{-17}$, n = 0.5
C_{pr}	coeff = $2.7*10^{-11}$, n = 1
C_{par}	coeff = $2.5*10^{-11}$, n = 0.9

Table 6-4 Values of extracted parameters for Case I and II

Fig 6-14(a) shows the simulated plots of the impedance in Case I, i.e. Z_{m1} and Z_{c1}. The relative weighted least-square-errors of the magnitude and phase angle predictions of Z_{m1} are 0.006 and 0.088, respectively[52]. This plot can be compared with that of Fig 6-12(a) which is a plot of experimentally measured values. Similarly, Fig 6-14(b) shows the plot of Zm2 in Case II. Zc2 has not been demonstrated in Fig 10(b) since we have not modeled the cells adhered onto the passivation layer.

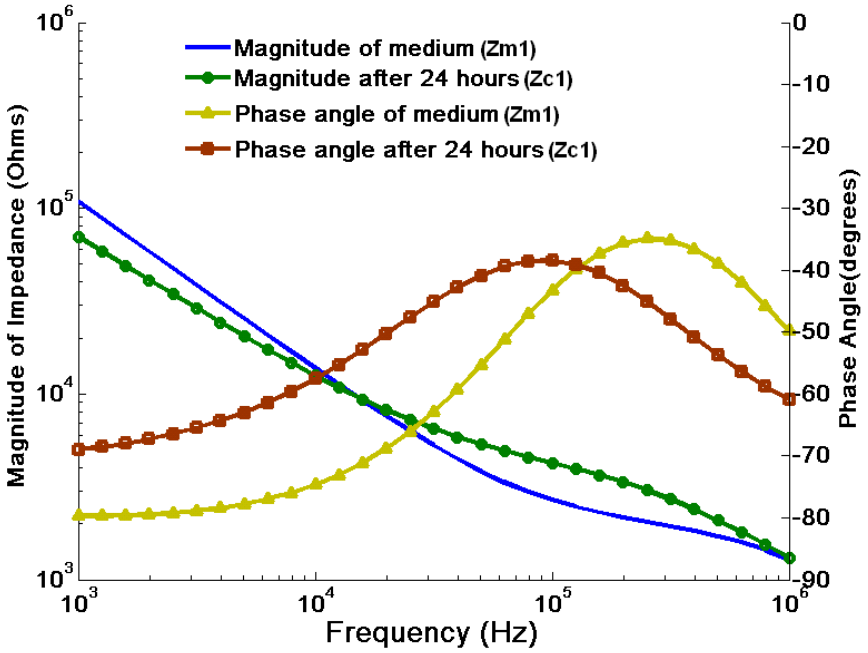

(a)

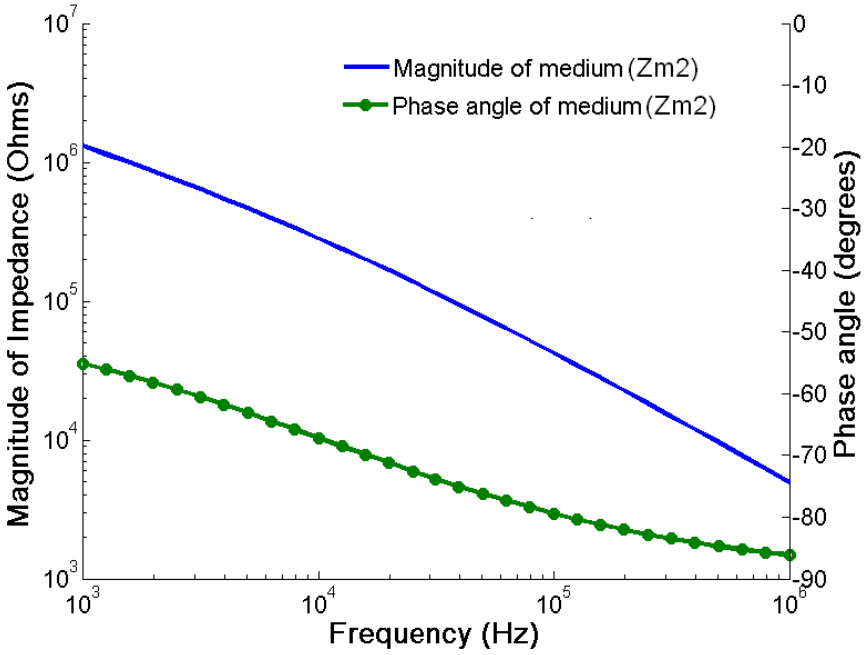

(b)

Fig 6-14 (a) shows the simulated impedance of the medium, in the presence and absence of cells in Case I while (b) simulates Z_{m2} which is for Case II, based on the parameters extracted from measurements.

Based on these parameters, the simulated values of normalized impedance for two different thicknesses (Γ_1 and Γ_{actual}) have been shown in Fig 6-15. The lower plot in Fig 6-15 corresponds to the test condition for photoresist thickness. The drop in the amplitude for the simulated case is 8% based on the model. This confirms our earlier observation shown in Fig. 9, that the sensitivity of the sensor (Γ_{actual}) was reduced due to the non-ideal presence of the passivation layer. However, the difference between the simulated and experimental results (13%) is due to the minute errors in the extracted parameter values. The plot of Γ_1, at the center of Fig 6-15, corresponds to the case wherein the photoresist thickness is thrice more than the test case. It can be observed that the loss in sensitivity is reduced to about 3%.

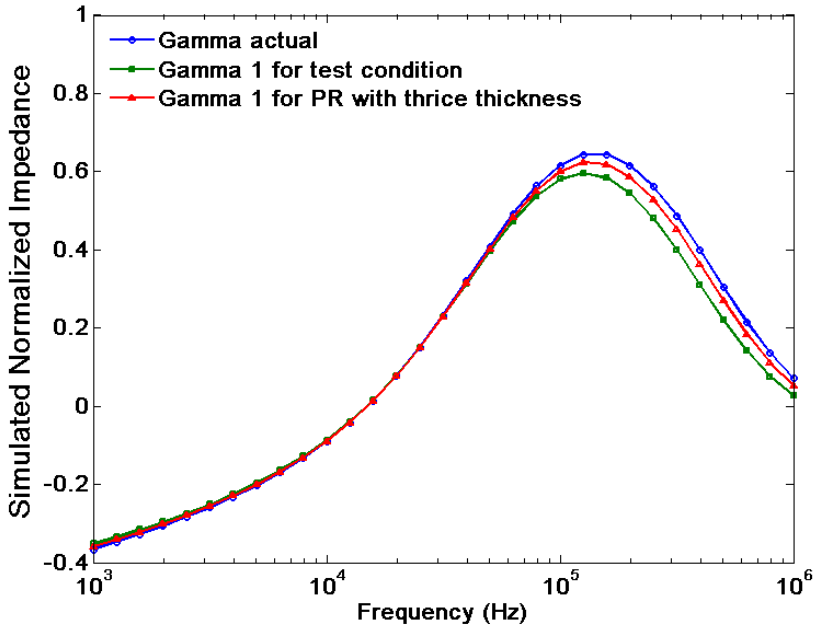

Fig 6-15 Simulated Γ_1 and Γ_{actual} have been plotted for the impedance measured after 24 hours and closely matches the measured plot in Fig. 9. The Γ_1 for the test case and a case with photoresist with thrice the thickness have been plotted. The latter shows a lesser loss in sensitivity.

The non-linear effect of the passivation layer noted in the previous section can be explained based on Fig 6-16, wherein two impedance measurements have been plotted, Z_s and Z_p. The impedance of the medium measured in Case II, Z_{m2}, can be approximated to Z_p. Similarly, the impedance of the medium measured in Case I, Z_{m1}, can be approximated to Z_s. This approximation is reasonable due to the large difference in Z_{m1} and Z_{m2}. The frequency spectrum can be split into two regions. In region 1, since Z_p is an order of magnitude larger than Z_s, Z_p does not affect Z_s and hence the decrease in sensitivity is negligible. However, in region 2, as the impedance increases due to the presence of cells on the sensing window, Z_s is increasingly comparable to that of Z_p. The parallel combination of Z_s and Z_p is significantly smaller than Z_s. The increase in the impedance is lower than what it has to be. Hence the normalized graph shows a smaller peak.

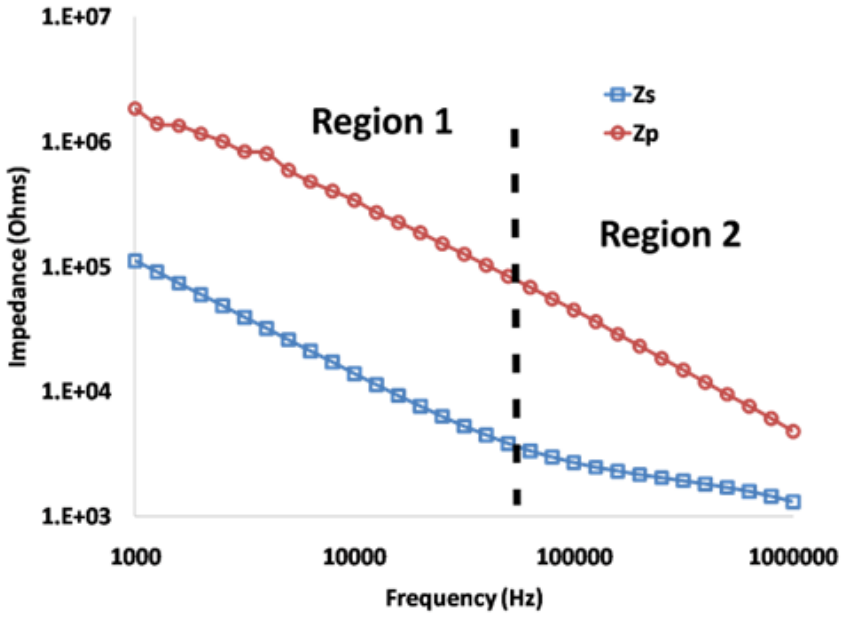

Fig 6-16 A plot to compare the relative values of Zs and Zp at different frequencies in the absence of cells.

7 Conclusion and Future Work

In this research, we concentrated on MDA-MB-231 cells. Impedance was measured in the absence and presence of cells, modeled and studied for the variation over time. The normalized impedance was projected as a useful parameter in observing the attachment of cells. However, the measurements are not correlated with any real-time imaging of cells on the surface. Visual observation based analysis of cells is the time-tested procedure followed by biologists. It is thus imperative to relate the impedance measurement against some visually observable feature. This relation will help in deploying the sensor as a viable tool in cell-analysis. In the modeling section, the impedance due to the cell has been modeled as a parallel RC circuit without relating it to any physical characteristic of the cell such as cell-substrate gap resistance, solution capacitance, membrane capacitance. This needs to be investigated and will fill the void described in the previous statements. The impedance measurements reported in this research are for electrodes whose effective diameter is more than 100µm. Measurements on smaller electrodes can have a larger variation due to fabrication mismatches.

In spite of the various planar-designs reported in literature, it should be noted that the selectivity of the sensor to a particular cell type of a co-culture has not been established. The reason partly lies in the fact that different cell types that adhere onto surfaces do not show a huge variation when exposed to a planar surface. The key will be to micro-engineer the surface (structural engineering) to a degree that can be sensed by the cells to obtain a huge sensitivity. Selectivity obtained by impedance measurement and structural engineering need not be independent. With individual cell lines, non-planar structures could give different electrical signals, due to the morphological changes in the cells.

Apart from impedance measurement characterization, the effect of the passivation layer has been quantified. To reduce the effect of the passivation layer the impedance of the passivation layer (Z_p) needs to be increased. Employing a passivation layer with lower dielectric constant is a possibility provided the replacement material is bio-compatible. However, the dielectric constant for photoresist is around 2.7 [24]. Polyimide has a similar dielectric constant, can be spun for larger thicknesses and is widely regarded as a superior bio-compatible than photoresist and would be a better choice for future experiments.

REFERENCES

1. Vassos, B. and G. Ewing, *Electroanalytical chemistry*. 1983: Wiley New York.
2. Huang, X., et al. *Development of active matrix biosensor array for cell screening*. 2004.
3. Giaever, I. and C. Keese. *Monitoring fibroblast behavior in tissue culture with an applied electric field*. 1984: National Acad Sciences.
4. Goda, N., et al. *Evaluation of the electrical cell-substrate impedance sensing system (ECIS) method using a mathematical model*. 2004.
5. Ehret, R., et al., *Monitoring of cellular behaviour by impedance measurements on interdigitated electrode structures.* Biosensors and Bioelectronics, 1997. **12**(1): p. 29-41.
6. Robinson, D.A., *The electrical properties of metal microelectrodes.* Proceedings of the IEEE, 1968. **56**(6): p. 1065-1071.
7. Wise, K.D. and J.B. Angell, *A Low-Capacitance Multielectrode Probe for Use in Extracellular Neurophysiology.* Biomedical Engineering, IEEE Transactions on, 1975. **BME-22**(3): p. 212-219.
8. Gross, G.W., *Simultaneous Single Unit Recording in vitro with a Photoetched Laser Deinsulated Gold Multimicroelectrode Surface.* Biomedical Engineering, IEEE Transactions on, 1979. **BME-26**(5): p. 273-279.
9. Kuperstein, M. and D. Whittington, *A practical 24 channel microelectrode for neural recording in vivo.* IEEE Transactions on Biomedical Engineering, 1981: p. 288-293.
10. Giaever, I. and C. Keese, *Behavior of cells at fluid interfaces.* Proceedings of the National Academy of Sciences, 1983. **80**(1): p. 219.

11. Nguyen, D., et al., *Fibroblast growth and H-7 protein kinase inhibitor response monitored in microimpedance sensor arrays.* Biotechnology and bioengineering, 2004. **87**(2).

12. Giaever, I. and C. Keese, *Use of electric fields to monitor the dynamical aspect of cell behavior in tissue culture.* IEEE Transactions on Biomedical Engineering, 1986: p. 242-247.

13. Giaever, I. and C. Keese, *Micromotion of mammalian cells measured electrically.* Proceedings of the National Academy of Sciences, 1991. **88**(17): p. 7896-7900.

14. Keese, C., et al., *A biosensor that monitors cell morphology with electrical fields.* IEEE Engineering in Medicine and Biology Magazine, 1994. **13**(3): p. 402-408.

15. Huang, X., et al. *Impedance based biosensor array for monitoring mammalian cell behavior*. 2003.

16. Keese, C. and I. Giaever. *A whole cell biosensor based on cell-substrate interactions*. 1990.

17. Izzard, C. and L. Lochner, *Formation of cell-to-substrate contacts during fibroblast motility: an interference-reflexion study.* Journal of Cell Science, 1980. **42**(1): p. 81.

18. Mitra, P., C. Keese, and I. Giaever, *Electric measurements can be used to monitor the attachment and spreading of cells in tissue culture.* Biotechniques, 1991. **11**(4): p. 504-510.

19. Giaever, I. and C. Keese, *Cell substrate electrical impedance sensor with multiple electrode array*. 1993, Rennselaer Polytechnic Institute, Troy, N.Y.

20. Lo, C., C. Keese, and I. Giaever, *Impedance analysis of MDCK cells measured by electric cell-substrate impedance sensing.* Biophysical journal, 1995. **69**(6): p. 2800-2807.

21. GIAEVER, I. and C. KEESE, *A biosensor that monitors mammalian cells with electrical fields*, in *Physics of biomaterials: fluctuations, selfassembly, and evolution*. 1996. p. 173.

22. Lo, C., C. Keese, and I. Giaever, *Cell–substrate contact: another factor may influence transepithelial electrical resistance of cell layers cultured on permeable filters.* Experimental Cell Research, 1999. **250**(2): p. 576-580.

23. GIAEVER, I. and C. KEESE, *Attachment and spreading of mammalian cells in vitro*, in *Soft Condensed Matter: Configurations, Dynamics and Functionality*. 2000. p. 101.

24. Wegener, J., C. Keese, and I. Giaever, *Electric cell-substrate impedance sensing (ECIS) as a noninvasive means to monitor the kinetics of cell spreading to artificial surfaces.* Experimental Cell Research, 2000. **259**(1): p. 158-166.

25. Greve, D., et al. *Modeling of impedance of cell-covered electrodes*. 2003.

26. Huang, X., et al. *Impedance-based Biosensors*. 2004.

27. Nguyen, D. *Impedance Array Studies of Mammalian Cell Growth*. 2003: American Institute of Chemical Engineers.

28. Nguyen, D., et al. *Screening of isolated cells via arrays of impedance sensors*. 2003.

29. Huang, X., et al., *Simulation of microelectrode impedance changes due to cell growth.* IEEE Sensors Journal, 2004. **4**(5): p. 576-583.

30. Hofmann, M., et al., *Galvanic decoupled sensor for monitoring biomass concentration during fermentation processes.* Sensors & Actuators: B. Chemical, 2005. **111**: p. 370-375.

31. Hofmann, M.C., et al. *Galvanically decoupled impedance spectroscopy for biological high-throughput-screening in microtiter plates*. 2005. Irvine, CA, United states: Institute of Electrical and Electronics Engineers Inc.

32. Jianhui, L., et al. *Impedance Spectroscopy Analysis of Cell-Electrode Interface*. 2005.

33. Goda, N., et al. *Quantitative Evaluation of Micro-motion of Vascular Endothelial Cells in Electrical Cell-substrate Impedance Sensing (ECIS) Method Using a Precision Mathematical Model*. 2006.

34. Gomes, H., et al. *A microelectrode impedance method to measure interaction of cells*. 2004.

35. Radke, S. and E. Alocilja, *Design and fabrication of a microimpedance biosensor for bacterial detection.* IEEE Sensors Journal, 2004. **4**(4): p. 434-440.

36. Rahman, A., C. Lo, and S. Bhansali, *A micro-electrode array biosensor for impedance spectroscopy of human umbilical vein endothelial cells.* Sensors & Actuators: B. Chemical, 2006. **118**(1-2): p. 115-120.

37. Price, D., A. Rahman, and S. Bhansali, *Design rule for optimization of microelectrodes used in electric cell-substrate impedance sensing (ECIS).* Biosensors and Bioelectronics, 2008.

38. Instruments, G., *EIS Primer.* Gamry Instruments, Pennsylvania, 2007.

39. Grimnes, S. and O. Martinsen, *Bioimpedance and bioelectricity basics*. 2008: Academic press.

40. Plambeck, J., *Electroanalytical Chemistry: basic principles and applications*. 1982: Wiley New York.

41. Barsoukov, E. and J. Macdonald, *Impedance spectroscopy: theory, experiment, and applications*. 2005: Wiley-Interscience.

42. Muralidharan, V., *Warburg impedance-basics revisited.* Anti Corrosion Methods and Materials, 1997. **44**(1): p. 26-29.

43. Roach, K., *Electrochemical Models for Electrode Behavior in Retinal Prostheses. M. Eng*. 2003, Thesis, Massachusetts Institute of Technology, Department of Electrical Engineering and Computer Science.

44. Taylor, D. and A. MacDonald, *AC admittance of the metal/insulator/electrolyte interface.* Journal of Physics D: Applied Physics, 1987. **20**: p. 1277-1283.

45. Baca, A. and C. Ashby, *Fabrication of GaAs devices*. 2005: Iet.

46. Technologies, A., *Impedance measurement handbook.* Agilent technologies, Palo Alto, 2003.

47. Slade, P., *Electrical contacts: principles and applications*. 1999, New York: Marcel Dekker.

48. Nobel, P., *Physicochemical & environmental plant physiology*. 1999: Academic Pr.

49. Salvadori, M., et al., *Measurement of the elastic modulus of nanostructured gold and platinum thin films.* Physical Review B, 2003. **67**(15): p. 153404.

50. Ni, H., X. Li, and H. Gao, *Elastic modulus of amorphous SiO nanowires.* Applied Physics Letters, 2006. **88**: p. 043108.

51. Narayanan, S., et al. *Method to Quantify the Effect of Passivation Layer in Bio-Impedance Sensors*. in *31st Annual International Conference of the IEEE Engineering in Medicine and Biology Society (EMBC'09)*. 2009. Minneapolis, MN, USA.

52. Motulsky, H.J. and A. Christopolous, *Fitting models to biological data using linear and nonlinear regression. A practical guide to curve fitting*. 4.0 ed. 2003, SanDiego, CA: GraphPad Software Inc.

APPENDIX A

MATLAB Code used for curve fitting

%This is the program that was generated to extract cell paramters from 100µm electrode on 25th of Jan.

```
%Impedance calculator created on Jan 10th of 2009

elno=5;
area = pi*(300e-6/2)^2;                 %area of electrode in m^2
cells=true;

Rgapcoeff = 7.8e-4;
Rgap = Rgapcoeff/area;
Ccellcoeff = 0.52e-3;
Ccell = Ccellcoeff*area;;
m=.83;

npar=.76;
Cpar = 3.7e-11;                         %parasitic capacitance
n=.98;                                  %CPE exponent
Celcoeff_nc = 2.9e-2;                   %parameter from curve fit - constant
if(cells==true)
   Celcoeff = Celcoeff_nc*1.4;
else
   Celcoeff = Celcoeff_nc;
end
Cel= Celcoeff*area;
Rspcoeff = 4.2e-1;                      %parameter from curve fit - constant
Rsp= Rspcoeff/(area)^.5;

fmin=1e3;                               %min frequency in Hz
fmax=1e6;                               %max frequency in Hz
fnum=31;                                %number of points

if(cells == true)
   mag=xlsread('c:\mag.xls');
   ang=xlsread('c:\ang.xls');
else
   mag=xlsread('c:\mag_nc.xls');
   ang=xlsread('c:\ang_nc.xls');
end

%------------------------------------------------------------------------->
```

```
mag = mag(:,elno+1);
ang = ang(:,elno+1);
actual = mag.*exp(i*ang.*pi/180);

f=logspace(log10(fmin),log10(fmax),fnum);
w=2*pi.*f;

if (cells ==false)
   nocell = (((i.*w*Cel).^-n + Rsp ).^-1 + (i*Cpar.*w).^npar ).^-1;
else
   nocell = (((i.*w*Cel).^-n + (Rgap^-1 + (i.*w*Ccell).^m).^-1 + Rsp ).^-1 +
(i*Cpar.*w).^npar ).^-1;
end

subplot(2,1,1);loglog(f,abs(nocell),f,mag);
legend('Simulated','Measured');
subplot(2,1,2);semilogx(f,angle(nocell).*180/pi,f,ang);

%This one was for 200μm electrode area
```